A *TranSNP* in the DDIT4 mRNA can impact its translation efficiency and modulate p53-dependent responses in cancer cells

Meriem Hadjer Hamadou*[1], Laura Alunno*[1], Tecla Venturelli[1,2], Samuel Valentini[2], Davide Dalfovo[2], Francesca Lorenzini[3], Alessia Mattivi[4], Vincenza Vigorito[4], Glenda Paola Grupelli[5], Alessandro Matte'[6], Pamela Gatto[7], Michael Pancher[7], Chiara Valentini[8], Veronica De Sanctis[8], Roberto Bertorelli[8], Virginie Marcel[9], Emilio Cusanelli[5], Stefano Freddi[10,11], Giovanni Bertalot[12], Sara Zaccara[13], Marina Mione[3], Luca L. Fava[4], Alessandro Romanel[#2], Alberto Inga[#1]

[1] Laboratory of Transcriptional Networks; [2] Laboratory of Bioinformatics and Computational Genomics; [3] Laboratory of Experimental Biology;[4] Armenise-Harvard Laboratory of Cell Division; [5] Cell Biology and Molecular Genetics Laboratory; [6] Cell Analysis and Separation Core Facility; [7] High-Throughput Screening Core Facility; [8] Next Generation Sequencing (NGS) Core Facility; Department of Cellular, Computational, and Integrative Biology, CIBIO, University of Trento, via Sommarive 9, 38123, Trento, Italy

[9] Ribosome, Translation and Cancer » team, Centre de Recherche en Cancérologie de Lyon (CRCL), INSERM U1052, CNRS UMR5286, Centre Léon Bérard, Université de Lyon, Université Claude Bernard Lyon 1, 69008, Lyon, France

[10] Department of Oncology and Hematology-Oncology, Università degli Studi di Milano, Milan, Italy

[11] IEO, European Institute of Oncology IRCCS, Milan, Italy

[12] Unità Operativa Multizonale di Anatomia Patologica, APSS, Trento, Italy, Centre for Medical Sciences – CISMed, University of Trento, Italy

[13] Department of Systems Biology, Columbia University Irving Medical Center, NY, USA

* equal first authors
#equal last and corresponding authors

Abstract

Relatively few studies have examined the link between SNPs and mRNA translation, despite the established importance of translational regulation in shaping cell phenotypes. We developed a pipeline analyzing the allelic imbalance in total and polysome-bound mRNAs from paired RNA-seq data of HCT116 cells and identified 40 candidate tranSNPs, i.e. SNPs associated with allele-specific translation. Among them, the SNP rs1053639 (T/A) on DNA damage-inducible transcript 4 (DDIT4) 3'UTR was identified, with the reference T allele showing a higher polysome association. rs1053639 TT clones generated by genome editing exhibited significantly higher DDIT4 protein levels than AA ones. The difference in DDIT4 proteins was even greater when cells were treated with Thapsigargin or Nutlin, two perturbations that induce DDIT4 transcription. The RNA-binding protein RBMX influenced these allele-dependent differences in DDIT4 protein expression, as shown by RNA-EMSA, RIP, and smiFISH assays. RBMX depletion reduced DDIT4 protein in TT clones to the AA levels. Functionally, TT clones more effectively repressed mTORC1 under ER stress, while AA clones outcompeted TT clones in vitro or when injected in zebrafish embryos. RBMX depletion increased the fitness of TT cells in co-culture experiments. The rs1053639 AA genotype, under a recessive model, correlates with poor prognosis in TCGA cancer data.

Keywords

Polysome-profiling; translation; DDIT4, mTOR, p53, ER-stress

Key points

-Translatome analysis in HCT116 cells revealed allele-specific mRNA translation for 40 SNPs

-rs1053639 (T/A) in DDIT4 3'UTR showed allelic differences in mRNA localization & protein expression

-AA cells showed weaker mTOR inhibition & higher proliferation; AA individuals had poorer prognosis

Introduction

Many studies in the last decade have demonstrated the importance of translational regulation in shaping cell phenotype (1–4). Instead, relatively few studies focused on the identification and characterization of genetic variants impacting directly on mRNA translation, although allele-specific expression finely modulating epigenetic and transcriptional regulation has been revealed as critical for many pathophysiological processes (5–8). To investigate instances of allele-specific mRNA translation efficiency, we recently developed a method that focuses on single nucleotide polymorphisms (SNP) and integrates information from SNP genotyping with RNA-seq data performed on both total and polysome-bound mRNAs (9). Briefly, heterozygous SNPs mapped by genotyping assays are followed in RNA-seq data by calculating allelic fractions (AFs) for both total and polysomal RNA. Coverage threshold, consistency among biological replicates, and the differences in AF between paired total and polysomal RNA samples are used to nominate candidate tranSNPs. The method assumes that the translatome, defined as the ensemble of transcripts that co-sediment with polysomes on sucrose gradients, represents a proxy for the proteome (10). Also, it assumes that if two alleles expressed by a cell can be distinguished due to heterozygous SNPs or other types of variants, a difference in their relative abundance within the polysomes would signal an instance of allele-specific difference in translation efficiency. Hence, the name tranSNPs is attributed to the variants emerging from our pipeline (9). Besides polysomal profiling, Ribo-seq is another approach typically used to characterize the translatome. The method can reach a single-nucleotide positional resolution of the ribosomes along a transcript. The polysome-seq variant protocol could be potentially applied to our scope, as 80S monosomes, whose actual translational status is still somewhat debated (11), are removed before processing the samples by RNAse treatment to retrieve ribosome-protected fragments (12). However, we decided to use polysomal profiling to increase the possibility of obtaining robust coverage also in 5'- and 3'-UTR regions of mRNAs. Our earlier study identified 147 tranSNPs, corresponding to about 4% of analyzable SNPs in a dataset obtained in the MCF7 cancer cell lines. Of those, 39 were located in the 3'UTR (9) and could impact, directly or

through structural features, the binding of trans-factors that, in turn, can affect translation efficiency or mRNA stability.

We have now extended our analysis using data produced in the HCT116 p53 wild-type cell line cultured in control conditions or treated with the MDM2 inhibitor Nutlin (13). While tranSNPs could potentially impact multiple cellular phenotypes and outcomes, we decided to continue to focus on a non-genotoxic p53-activating treatment in cancer cells due to profound changes in mRNA translation in cancer (4), and the growing evidence linking the tumor suppressor p53 to various features of mRNA translation control. For example, p53 was shown to modulate eIF4EBP1, mTORC1, and Endoplasmic Reticulum (ER) stress (14–16), and, through the modulation of Ribosomal Proteins (RBPs) and microRNAs, to impact the fate of specific sets of mRNAs (17–19). We identified 40 candidate tranSNPs, corresponding to about 7% of analyzable SNPs. Among these tranSNP candidates, four were prioritized for validation experiments considering minor allele frequency, the relevance of the associated genes in cancer, the position along the gene sequence, and the presence of predictions for overlapping trans factor binding sites. One candidate, rs1053639 T/A in the 3'UTR of the DDIT4 (REDD1, RTP801) gene, caught our particular interest. DNA damage-inducible transcript 4 DDIT4 is a negative modulator of mTORC1, is an established target of p53, RFX7, and ATF4, and acts as a tumor suppressor gene (20,21). We generated HCT116 cell line trios for rs1053639 exploiting a CRISPR/Cas9-mediated knock-in strategy (22) starting from the heterozygous (AT) parental cells. Homozygous TT and AA cell clones were characterized, which revealed differences in DDIT4 protein expression both in basal and induced conditions, alterations in the relative expression of mTOR markers, and changes in mRNA subcellular localization and translatability. Mechanistically, we implicated the RNA binding protein RBMX in a distinct fate of DDIT4 mRNA for rs1053639 alleles. We also established higher relative proliferation and fitness for A-homozygous cells in both *in vitro* and xenograft experiments in zebrafish embryos and explored the correlation between rs1053639 alleles and DDIT4 protein expression in primary tumor samples and the prognostic value of this SNP using TCGA data.

54 # Results

55 **TranSNPs can be identified in mock and Nutlin-treated HCT116 cells**

56 Single-end RNA-seq data obtained from HCT116 cells under either mock or 10 μM Nutlin treatment
57 for 16 hours were processed starting from row files by trimming, aligning, and deduplication steps
58 (see Methods). SNPs in exonic and UTR regions were extracted from dbSNP. A list of heterozygous
59 SNPs was compiled based on AF values between 0.2 and 0.8 in at least one of the four replicates in
60 one of the two fractions sequenced (total and polysomal RNA), setting a minimal threshold of 20
61 reads for AF calculations (**Figure S1**). In addition, only the SNPs with AF measures available for all
62 four biological replicates, the two fractions, and across the two treatments were considered to
63 calculate changes in AF between the fractions (N= 582, **Table S1**). For each SNP, we exploited the
64 concordance among differential AF measures across pairs of polysomal and total RNA biological
65 replicates, performing paired statistics (**Figure S1**). This approach identified 40 putative tranSNPs
66 (**Figure 1A**), of which 21 are located in 3'UTRs (**Table S2**). Overall, we extended the methodology
67 previously developed (9) and observed that in HCT116, about 11% of genes with analyzable
68 heterozygous SNPs show a difference in AF between paired total and polysome-bound mRNAs,
69 suggesting allele-specific post-transcriptional and translational control.

70 Candidate tranSNPs for downstream analyses and validation were chosen considering
71 several SNP features (**Figure 1B, 1C**, **Table S1**, **S2**) and information about the associated genes.
72 Higher priority was given to SNPs with high magnitude of the AF imbalance, high minor allele
73 frequency (MAF), and positioned in 3'UTR of genes whose expression is altered in cancer or whose
74 function is associated with cancer-relevant features, especially p53-related. We selected a total of
75 four SNPs for validation (**Figure 1D-F, S1**). First, we sought to confirm differential allele-specific
76 expression found in polysomes versus total RNA. Sucrose gradient density sedimentation of
77 cytoplasmic lysates was performed (10), and fractions were collected and analyzed by UV
78 absorbance. RNA was recovered from the combined polysomal fractions and fractions corresponding
79 to ribosomal subunits and 80S monosomes. Total RNA was also extracted. Amplicons were
80 generated using primers specific for sequences surrounding the chosen SNPs (**Table S4**), Sanger

sequenced, and the electropherograms were analyzed, expressing the results as AF (alternative allele signal over the sum of alternative + reference allele signals), as done for the RNA-seq data. For three out of the four chosen SNPs, an imbalance consistent in direction with what was measured in the RNA-seq dataset was found (**Figure 1E, S1D, S1F**).

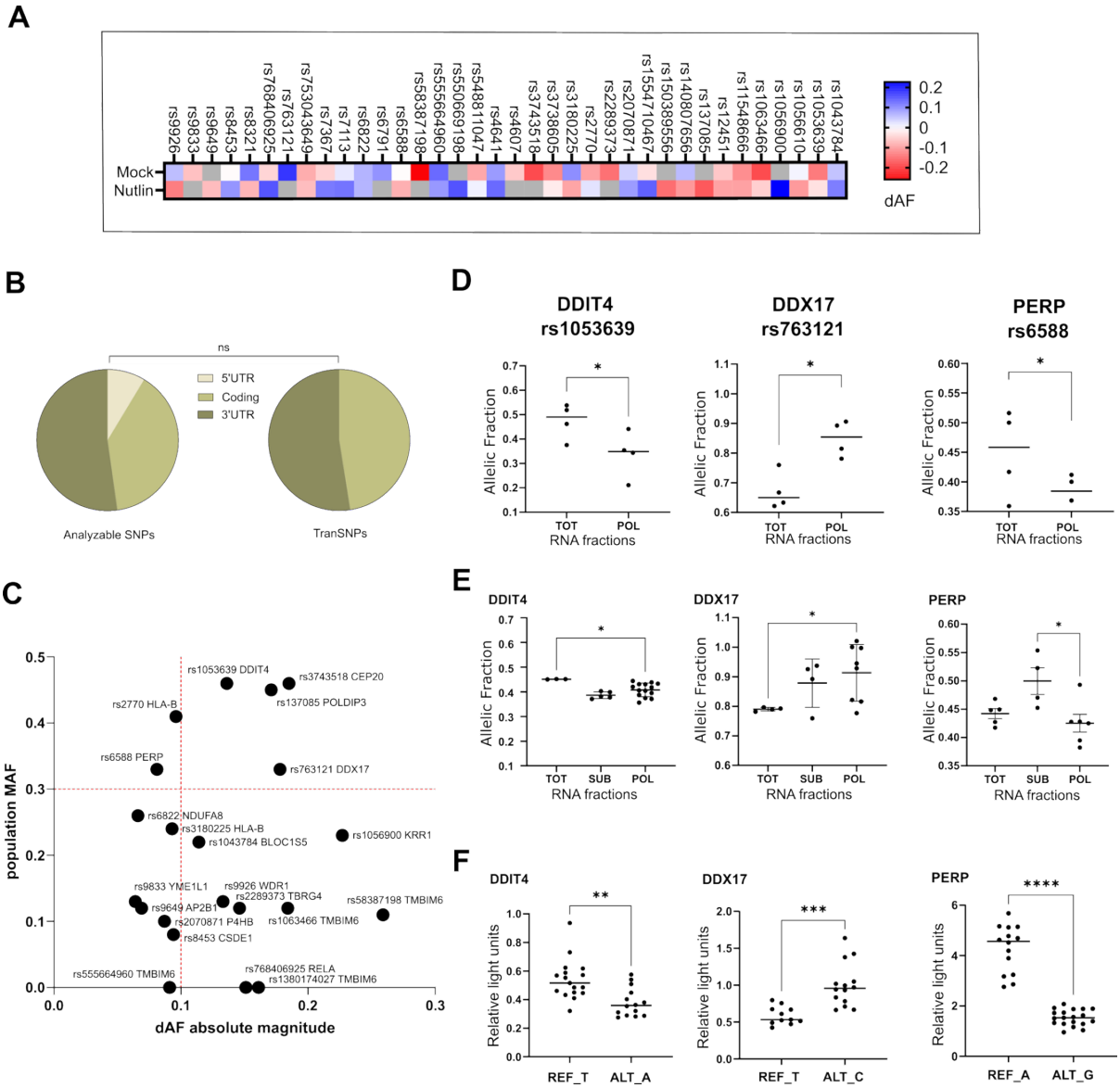

Figure 1. The tranSNPs in the DDIT4, DDX17, and PERP genes are validated by orthogonal approaches.

A) Heatmap view of average differences in allelic fractions (AF) in the comparison between polysome-associated and total RNA for the 40 tranSNPs identified from the RNA-seq data from either mock or Nutlin-treatment conditions (Tables S1 and S2 present the AF value for each biological replicate; accession number for the RNA-seq data: GSE95024). AF was computed as the number of reads for the alternative allele over the sum of reads of the alternative and reference alleles. **B**) Distribution across coding and regulatory regions of the transcripts for all analyzable SNPs (Left) and for the identified tranSNPs (Right). The result of Chi-square contingency test is shown. **C**) Plot presenting the absolute delta Allelic Fraction (dAF) and the Minor Allele Frequency (MAF) for the identified tranSNPs located in 3'UTRs. MAF values were derived from the 1000 Genomes Project Phase 3, all individuals. The SNP rsID and associated gene names are shown. **D**) Plots of the

AF for the rs1053639 (in DDIT4), rs763121 (in DDX17), and rs6588 (in PERP) tranSNPs obtained through RNA-seq of cytoplasmic total (TOT) and polysome-bound mRNAs (POL). Individual replicates and the AF mean are plotted. *p-value < 0.05, two-tailed, paired t-test. **E)** AF values of the selected tranSNPs calculated from Sanger sequencing electropherograms, comprising also the subpolysomal -RNP to 80S- (SUB) fractions. Individual replicates and the AF mean are plotted. *p-value < 0.05, two-tailed, paired t-test. **F)** Results of the dual luciferase assays presenting the relative activity (average and individual biological replicates) for the reference (REF_) and alternative (ALT_) alleles for each of the three selected tranSNPs cloned separately into the pGL4.13 vector immediately downstream of the Firefly luciferase stop codon. Data was normalized using Renilla luciferase. **p-value < 0.01. ***p-value < 0.001. ****p-Value < 0.0001, two-tailed, unpaired t-test.

We also used a targeted re-sequencing approach to measure allelic fractions from total and polysome-associated mRNAs, obtaining results consistent with the RNA-seq and Sanger sequencing (**Figure S1G**). Next, we asked whether the candidate tranSNPs could exhibit allele-specific differences in activity when extracted from their native context. To this aim, we cloned ~500 nt fragments of the 3'UTR sequences harboring those SNPs downstream of a luciferase plasmid reporter, using HCT116 genomic DNA. Given the heterozygous state of the cell line, we retrieved clones for both alleles for each SNP. Dual luciferase assays were then performed in HCT116 cells, with results further supporting the observation that the SNPs and their immediate surroundings are sufficient to show allele-specific differences in reporter activity (**Figure 1F, S1**).

Editing of HCT116 cells to obtain the three genotypes of rs1053639 tranSNP

It is worth noting that while the heterozygous state and the comparison of AF among two RNA compartments (total versus polysomal) are necessary to enable reliable identification of tranSNPs in our approach, we expect that the homozygous state for alternative and reference alleles would reveal the highest level of phenotypic impact of this category of genetic variants. Hence, our next step was constructing potentially isogenic cell clones by CRISPR/Cas9-mediated editing. We exploited the CRISPR/Cas9-mediated knock-in delivering the Cas9 and the guide RNA (gRNA) as a ribonucleoparticle (RNP) to reduce its off-target potential (22) (**Figure S2A**). Based on the collective RNA-seq, validation data, editing amenability, and the relevance of the gene in cancer, including its functional links with p53 (20,23,24), the T/A rs1053639 in DDIT4 was a promising tranSNP. HDR efficiency by the ICE Synthego analysis web tool (26) ranged from 5% to 9% for the initial bulk populations. 85 clones were isolated and characterized by Sanger sequencing. We obtained at least

129 four clones homozygous for the rs1053639 T allele and four homozygous for the A allele. However,
130 three clones (#3 TT, #5, and #6 AA) contained the same GGT 3 nt deletion, starting three nucleotides
131 after the SNP site. We also obtained two clones bearing either a 9-nucleotide deletion (#7) or a 29-
132 nucleotide deletion (#8) encompassing the SNP position (**Table S6**, **Figure S2B,** and methods). We
133 considered at least two clones among the rs1053639 TT (#2, #3, #12, #13), and AA (#5, #6, #7, #10)
134 along with the unedited AT clone (#1) to overcome the potential influence of clonal selection and
135 adaptation and the above-mentioned editing limitations. We then used these cell models to study the
136 SNP effect on various phenotypic assays.
137
138 **Higher DDIT4 protein levels in rs1053639 TT homozygous clones**
139 First, we tested the impact of the tranSNP status on DDIT4 steady-state protein levels (**Figure 2A,**
140 **B**). TT clones exhibited significantly higher relative protein expression than AA clones, with the AT
141 cells intermediate. This result was consistent with the change in AF from RNA-seq or Sanger
142 sequencing that showed lower A allele representation in the polysomal fraction. The difference in
143 protein levels was not dependent on changes in protein half-life (**Figure 2C**), nor on mRNA levels
144 and turnover (**Figure 2D**). An antisense DDIT4-AS1 transcript corresponding to the 3'UTR region
145 was reported to affect the stability of the DDIT4 transcript (27,28). However, DDIT4-AS1 was
146 equally expressed across TT and AA clones, and its expression was significantly lower than that of
147 the DDIT4 transcript (**Figure 2E**). Next, we challenged the cells with Thapsigargin (100nM for 4
148 hours) (29,30), an ER stressor (31) that is a strong inducer of DDIT4 expression (**Figure 2F**). As
149 expected, the treatment led to the marked induction of DDIT4 protein levels (**Figure 2G, 2H**).
150 Notably, the difference in expression associated with the SNP genotype was maintained, and the
151 lower expression of DDIT4 in AA clones was even more apparent. DDIT4 is also a recognized
152 transcriptional target of p53, directly or through the transcription factor RFX7 (20,24). Hence, we
153 examined whether the rs1053639 alleles differed in DDIT4 expression, also in response to p53
154 activation. Results showed that while the MDM2 inhibitor Nutlin led to comparable induction of p53
155 protein across the HCT116 DDIT4 clones, the associated induction in DDIT4 protein was higher for

the TT homozygous clones and intermediate for the AT cells (**Figure S3A-S3C**). AA clones did not show significant DDIT4 induction in response to Nutlin.

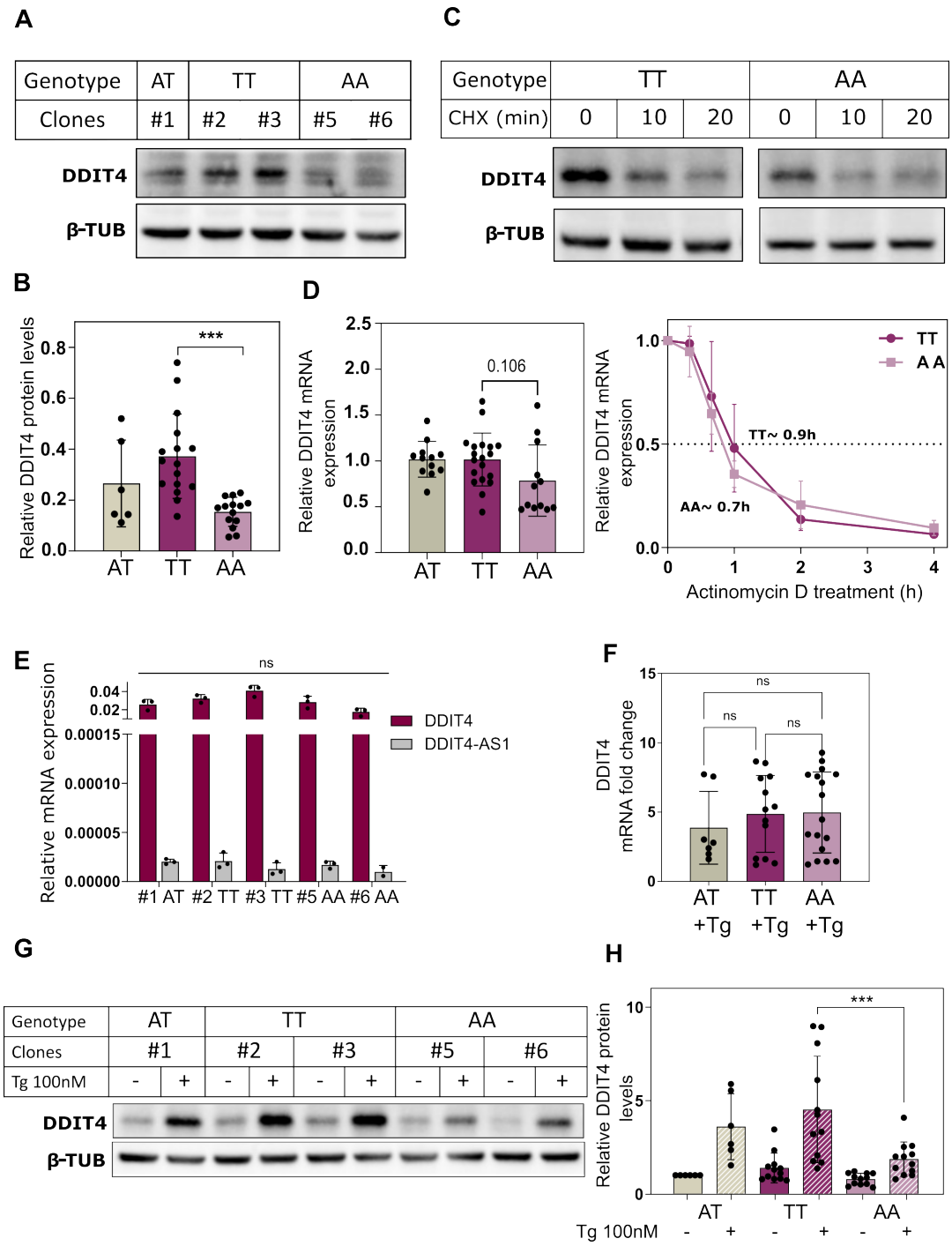

Figure 2. rs1053639 tranSNP impacts DDIT4 protein expression in HCT116-derived cells with the three genotypes.

HCT116 cells were edited by CRISPR/Cas9 RNPs and donor DNA to obtain cell trios with the three genotypes for the rs1053639 tranSNP located in the proximal portion of the DDIT4 3'UTR. **A)** Western blot analysis of

DDIT4 protein expression in HCT116 cells (A/T heterozygous) and DDIT4 rs1053639 homozygous clones (TT, AA). β-Tubulin was used as a reference. **B)** Densitometry analysis of the blots from several biological replicates shows a significant difference in relative DDIT4 protein abundance with the different tranSNPs genotypes. ***P-value <0.001, Ordinary one-way ANOVA. **C)** Western blot analysis of DDIT4 protein in HCT116 TT and AA homozygous clones for the rs1053639 treated with 100µg/ml cycloheximide (CHX) at the indicated time points. β-Tubulin was used as a reference. **D)** (Left) Relative DDIT4 mRNA expression as measured by RT-qPCR and normalized to GAPDH and YWHAZ. The Student's t-test showed no significant differences in DDIT4 mRNA expression in the different clones. ns, not significant. (Right) Estimation of DDIT4 mRNA stability following inhibition of transcription by actinomycin D treatment (10µg/ml). The curve presents the residual relative DDIT4 mRNA levels (average and standard deviation of at least three biological replicates) at various treatment time points measured by RT-qPCR decay from HCT116 clones harboring TT or AA genotypes. The estimated half-lives of the DDIT4 mRNA in TT and AA homozygous clones are indicated. **E)** DDIT4-AS1 and DDIT4 mRNA levels measured by RT-qPCR and normalized to GAPDH across TT and AA clones. The expression of DDIT4-AS1 was negligible compared to the expression of the sense DDIT4 mRNA in our cellular models. Data represents the mean ± SD of three independent experiments. ns, not significant. **F)** HCT116 clones were exposed to 100 nM thapsigargin (Tg) or vehicle for 4 hours, and the induction of DDIT4 mRNA was measured by RT-qPCR with clones of the three rs1053639 genotypes. Average, standard deviation, and individual replicates are presented. ns, not significant, student's t-test. **G-H**) Western blot and densitometry analysis showing relative DDIT4 protein induction upon thapsigargin (Tg 100nM) treatment of the three rs1053639 genotypes. β-Tubulin served as a control. ***p-value <0.001, unpaired t-test.

Since we observed higher polysomal association and higher DDIT4 protein levels from the rs1053639 T over the A allele, we examined at higher resolution the relative DDIT4 mRNA distribution across the sucrose gradient. For this experiment, RNA was recovered from ten individual fractions along the polysome profile (fractions 3 to 12, **Figure S4A**), and the DDIT4 mRNA distribution, along with CDKN1A and RPS26 controls, was measured by qPCR. Results were plotted as relative abundance, as previously described (32). In the mock condition, no significant differences in apparent translation efficiency for the DDIT4 mRNA between TT and AA homozygous cells were observed (**Figure 3A**).

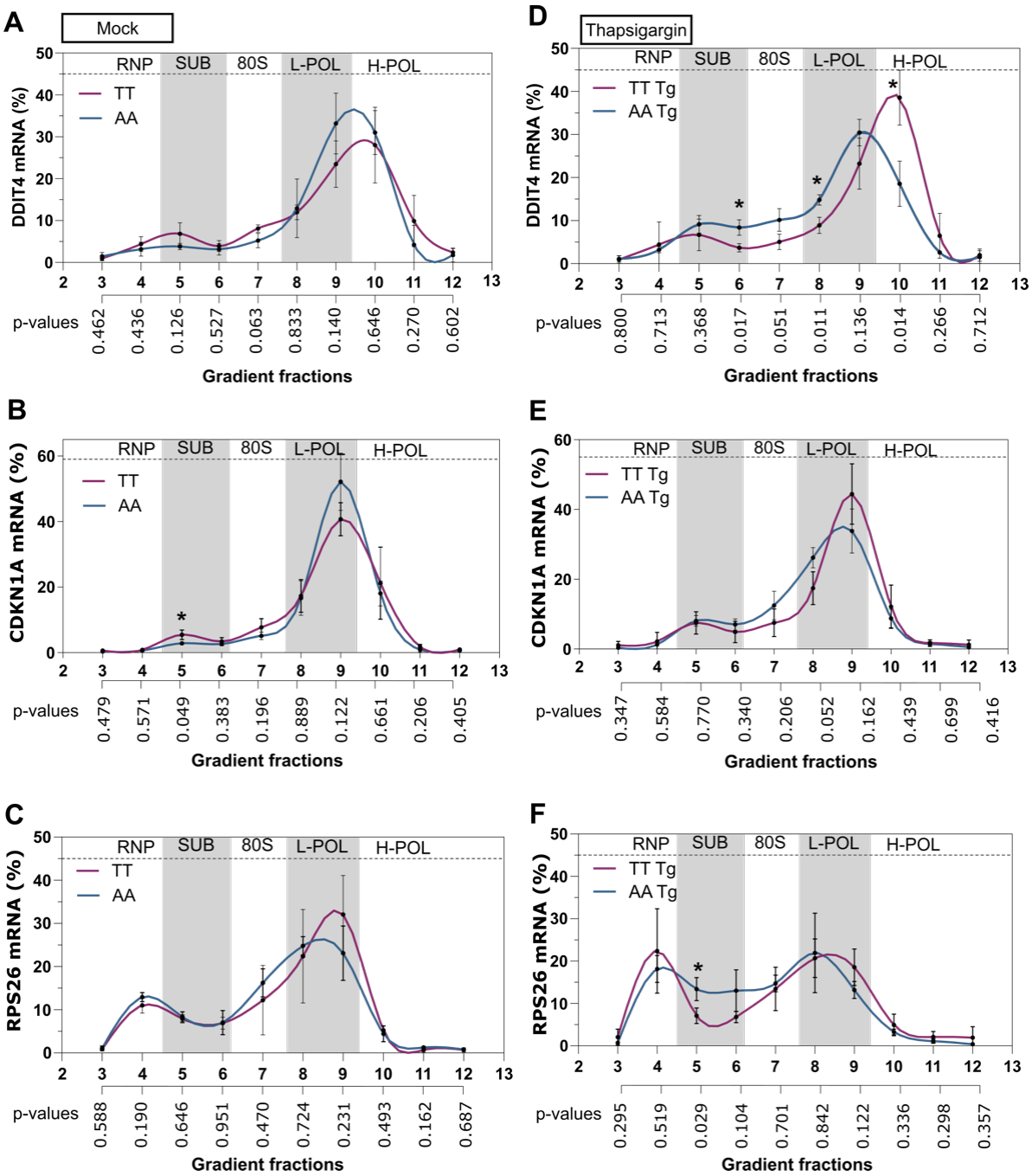

Figure 3. DDIT4 rs1053639 impacts its own mRNA distribution in polysomes.
Cytoplasmic lysates from HCT116 rs1053639 homozygous (TT, AA) clones treated with thapsigargin 100nM or vehicle for four hours were subjected to fractionation through sucrose density gradients (15 to 50%). Polysome profiles are shown in Figure S4A. **A-D**) The distribution of DDIT4 mRNA (mock or thapsigargin conditions) across the ten gradient fractions was analyzed across the two genotypes by RT-qPCR. The relative mRNA percentage in each fraction was plotted. Three independent biological experiments were performed. Presented are the average proportion and the standard deviations of the three replicates. Statistically significant p values at the unpaired t-test are indicated by an asterisk. The p-values are shown below the images. The shading pattern in each image refers to the sucrose-gradient fractionations (Figure S4A). RNP = light fraction corresponding to free RNA and ribonucleoprotein complexes; SUB = ribosomal subunits; 80S = monosomes. Fractions corresponding to the light (L-POL) and heavy polysomes (H-POL) are also highlighted. CDKN1A (**B-E**) and RPS26 (**C-F**) mRNAs were used as control transcripts and were analyzed using the same methodology as described for the DDIT4 mRNA.

211 No differences were also apparent for the CDKN1A and RPS26 mRNAs, except for a slight
212 increase in the proportion of CDKN1A in subpolysomal fraction 5 in TT cells (**Figure 3B, 3C**). When
213 the same analysis was performed after thapsigargin treatment, a shift was visible for the DDIT4
214 mRNA in TT cells, with significant higher proportion in polysomal fraction ten and corresponding
215 reduction in subpolysomal and light polysomal fractions, significant for fraction 5 and 8 (**Figure 3D**)
216 Thapsigargin treatment led to a general reduction in the polysome association for the three mRNAs,
217 which was more pronounced for the RPS26 mRNA (**Figure 3E, 3F**). A higher proportion of RPS6
218 mRNA in subpolysomal fraction 5 in AA cells was observed. Collectively, these results are consistent
219 with the higher DDIT4 protein expression in TT cells, particularly in response to thapsigargin
220 treatment.
221
222 **The rs1053639 tranSNP genotype impacts DDIT4 mRNA fate through the RBMX protein**
223 We developed predictions for allele-specific binding starting from a list of 552 RNA binding proteins
224 (RBPs) with consensus binding motifs (33), using the TESS software (DOI:10.1002
225 /0471250953.bi0206s21) (34) (**Table S3**). The predictions and the allele-specific binding scores
226 pointed to ACO1, YBX1, and particularly RBMX as RBPs that might differentially bind to the T/A
227 alleles. Recent PAR-CLIP data in HEK293T cells (35) highlighted that RBMX binds in the 3'UTR
228 of DDIT4 mRNA; therefore, we decided to focus on this target RBP. RBMX is mainly nuclear
229 located, can interact with structural features of mRNAs, and was reported to modulate mRNA
230 splicing, processing, and degradation (36–39). Hence, we performed RNA electromobility shift
231 assays using the full-length recombinant RBMX protein and RNA probes mimicking the secondary
232 structure of T and the A alleles of the endogenous DDIT4 mRNA. For the RNA probe design, we
233 took advantage of three learning-based methods (EternaFold, CONTRAfold, and Ufold), two
234 thermodynamic-based methods (ViennaRNA and RNAstructure), and one hybrid method (MXFold2)
235 (40–43). Although the global structure of the 3'UTR was not significantly impacted, significant
236 differences in the local secondary structure were observed after changing the base at the SNP site.
237 RNA EMSA revealed that both RNA probes are bound by RBMX *in vitro*, with a possible preference
238 for the T allele (**Figure 4A**). We further explored the publicly available web service AlphaFold 3 to

generate accurate structure predictions for protein-RNA interactions. Interestingly, AlphaFold 3 provided several models confirming that the T allele RNA EMSA probe is located in a more favorable spatial conformation than the A allele probe for RBMX binding (**Figure S5A**). It also predicts that the C-terminal low complexity domain of RBMX binds to DDIT4 mRNA.

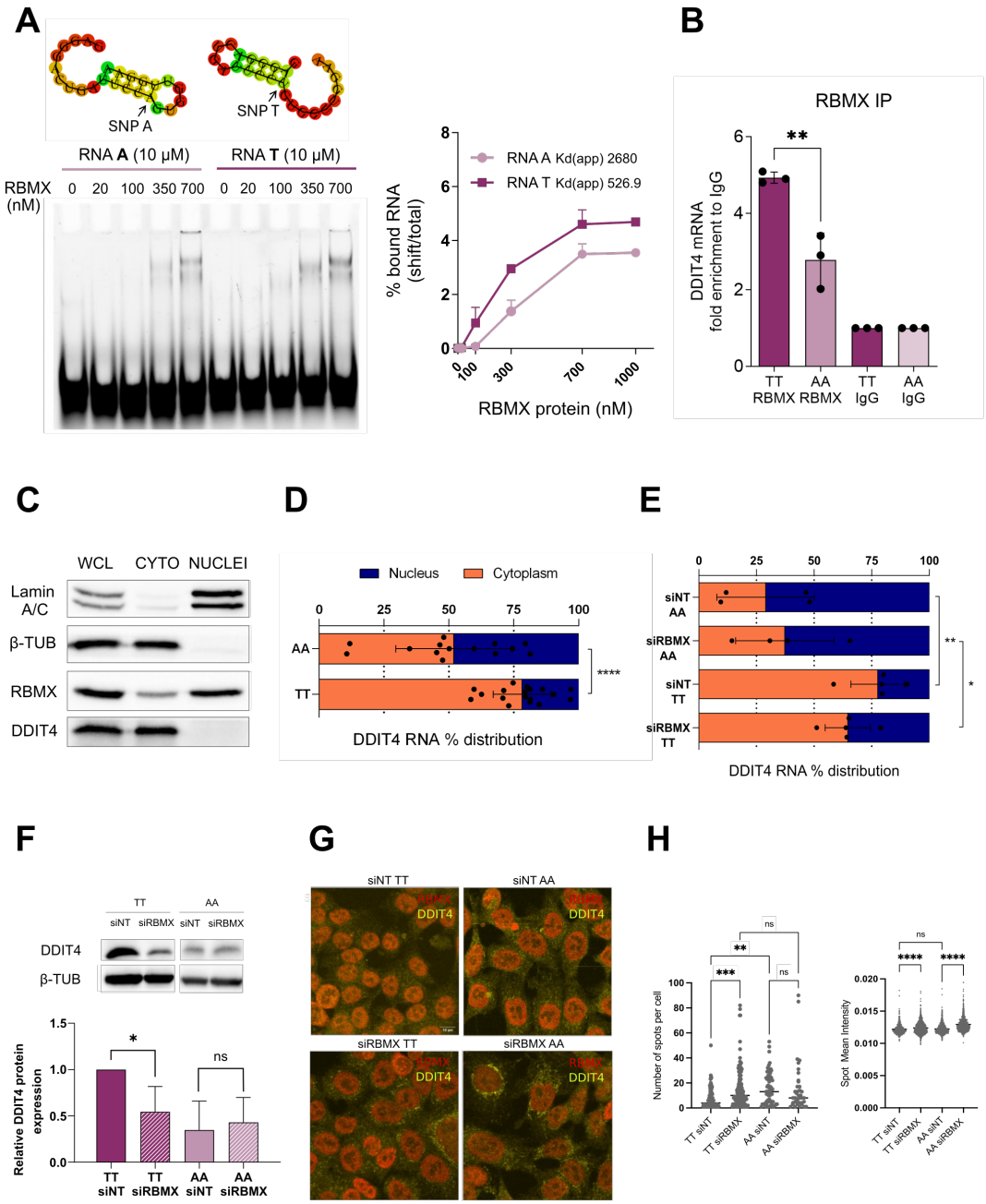

Figure 4. The rs1053639 tranSNP genotype impacts mRNA fate through the RBMX protein.
A) Left panel, structural RNA probes were designed based on RNA folding prediction tools on the endogenous DDIT4 3'UTR sequence. RNA EMSA was performed using the full-length recombinant RBMX protein and the above-mentioned RNA probes. In the '0' lane, the RNA probe was incubated with the binding buffer and the protein elution buffer. RNA-protein complexes were resolved on a native 6% gel. Right panel, quantification of the shifted bands in the REMSA experiments. Error bars plot the standard deviations among replicates. The apparent Kds obtained using non-linear regression fit are shown. **B)** The endogenous RBMX

251 protein was immunoprecipitated from a whole cell lysate in TT and AA clones. Results are expressed as fold
252 enrichment of the target DDIT4 mRNA relative to IgG. Three independent biological replicates were performed
253 **p-value < 0.001**,** unpaired t-test. **C)** Cell fractionation was performed in HCT116 cells, and protein levels
254 were evaluated. Lamin A/C (70-75 kDa) was used as a marker of the nuclear fraction, and β-Tubulin (55 kDa)
255 was used as a marker of the cytoplasmic fraction. The DDIT4 protein was found exclusively in the cytoplasm.
256 RBMX is mostly a nuclear protein, as previously reported. WCL: whole cell lysate. CYTO: cytoplasm. **D)**
257 RNA levels were evaluated in TT and AA cells upon cell fractionation, followed by RT-qPCR. The distribution
258 of DDIT4 mRNA is significantly different among TT and AA cells, with DDIT4 mRNA from TT cells being
259 considerably more enriched in the cytoplasm. Data represent the mean ± SD of at least four independent
260 experiments. The relative expression of the gene in the cytoplasm is calculated as the fold change of the Ct in
261 the cytoplasm compared to the Ct in the nucleus, with nuclear and cytoplasmic RNAs eluted in the same volume
262 of water. ****p-value < 0.0001. Unpaired t-test. **E)** DDIT4 mRNA levels in control (siNT) and in RBMX
263 knocked-down (siRBMX) TT and AA cells were evaluated upon cell fractionation and RT-qPCR. The
264 cytoplasmic localization of DDIT4 mRNAs was slightly reduced by RBMX depletion. Data represent the mean
265 ± SD of three independent experiments. *p-value = 0.0114 **p-value = 0.0031, unpaired t-test. **F)** DDIT4
266 protein levels in control (siNT) and RBMX knocked-down (siRBMX) TT and AA cells were evaluated upon
267 cell fractionation, followed by western blot. Representative blot of DDIT4 protein levels across TT and AA
268 clones (Top). Densitometry analysis of the blots from several biological replicates shows that DDIT4 protein
269 levels in TT clones decrease to the levels of the AA clones upon RBMX knockdown (Bottom). *p-value <
270 0.05, unpaired t-test. **G)** Confocal images of smiFISH-IF of a TT and an AA cell clone after control (siNT) or
271 RBMX silencing for 72 hours. RBMX protein is shown in red, and DDIT4 mRNA is shown in yellow. Scale
272 bar is 10 µm. **H)** At least three fields (15-20 cells per field) for each coverslip and each condition were imaged,
273 and cytoplasmic spots were quantified using Cell-Profiler 4.0.7 (Broad Institute, Inc.) and segmented as objects
274 with a typical diameter range of 10 to 30 pixels. (Left panel), number of DDIT4 mRNA spots per cell. (Right
275 panel), spot mean intensity. ** p< 0.01; *** p<0.001; **** p<0.0001, ordinary one-way ANOVA. ns = not
276 significant.

277

278 We then performed RIP assays to evaluate this interaction in a cellular context. The antibody used
279 proved to be effective for the RIP protocol (**Figure S5B**). We first performed RIP in parental HCT116
280 cells, followed by Sanger sequencing of the input and IP samples. However, we could not appreciate
281 quantitative differences in RBMX binding across the two alleles with this assay (**Figure S5C**). We
282 next used both the rs1053639 TT and AA clones to perform RIP-qPCR. The qPCR analysis revealed
283 that RBMX binds to DDIT4 mRNA slightly less than the positive control CSDE1, and we could
284 confirm the preferential binding to the rs1053639 T allele (**Figure 4B**). Given the nuclear localization
285 of RBMX and its binding to DDIT4 mRNA, we decided to examine the relative subcellular
286 localization of DDIT4 mRNA alleles. Specifically, nuclear and cytoplasmic fractions were obtained
287 and verified at both protein (**Figure 4C**) and RNA levels (**Figure S5F**). Results indicate that the
288 DDIT4 mRNA shows higher cytoplasmic localization in the TT clones while being significantly more
289 nuclear in the AA ones (**Figure 4D**). To shed light on the contribution of RBMX to this phenotype,
290 we confirmed that our edited cells expressed it at comparable levels, and we used siRNAs to deplete

291 its expression by ~50% (**Figure S5D, S5E**). Nuclear and cytoplasmic fractions upon RBMX silencing
292 were verified at the RNA level (**Figure S5G**). RBMX silencing led to a slight increase of nuclear
293 DDIT4 mRNAs in TT clones (**Figure 4E**), and, importantly, to a significant decrease of DDIT4
294 protein levels (**Figure 4F**). No significant changes were observed in AA cells. Single-molecule FISH
295 showed a punctuated distribution of the DDIT4 mRNA, particularly in the perinuclear region of the
296 cytoplasm (**Figure 4G, S5H**). The number of granules per cell was higher in the AA compared with
297 the TT clones (**Figure 4H,** left panel), while the spot mean intensity and area were not significantly
298 different across clones (**Figure 4H,** right panel**; S5I**). Interestingly, the depletion of RBMX led to a
299 significant increase in granularity in TT cells that reached the levels observed in the AA ones (**Figure**
300 **4G-H, S5I**). Hence, we suggest that RBMX contributes to the rs1053639 allele-specific regulation
301 of DDIT4 protein levels through multiple mechanisms that include export, cytoplasmic localization,
302 and translatability of the DDIT4 mRNA.
303
304 **The rs1053639 tranSNP genotype impacts on mTOR pathway markers**
305 Since DDIT4 is an established inhibitor of mTORC1, (20,44,45) we next sought to investigate
306 whether the effect of rs1053639 on DDIT4 protein levels would impact features of the mTOR
307 pathway as well. In particular, we analyzed the levels of EIF4EBP1 and S6K phosphorylation both
308 in basal culture conditions and in response to Thapsigargin treatment. We observed unexpectedly
309 higher levels of relative phospho-eIF4EBP1 and phospho-S6K for TT clones in basal conditions,
310 suggesting that our clones may have acquired compensatory mechanisms to balance their metabolism
311 (**Figure 5A-D**) (46,47). Instead, in response to Thapsigargin treatment, TT clones were associated
312 with a significant reduction in those mTORC1-dependent phosphorylations, which was not changed
313 in the AA clones. While the AA clone #6 showed a distinct eIF4EBP1 phosphorylation pattern,
314 analysis on additional AA clones revealed that this feature was not attributable to the AA genotype
315 but only to this specific clone. Analysis of the protein levels of the ER stress response markers ATF4,
316 a transcription factor regulating DDIT4 expression (48,49) (**Figure 5E**), and of the transcript levels
317 of CHOP, spliced XBP1, and SESN2 (**Figure 5F**) did not reveal differences among HCT116 clones
318 with the three rs1053639 genotypes in response to Thapsigargin (**Figure 5G**).

We concluded that the rs1053639 SNP status does not broadly impact the activation of the ER-stress response upstream of DDIT4. Consistent with the effect of Thapsigargin treatment, a more pronounced reduction in phospho-eIF4EBP1 was observed for TT homozygous cells also in response to Nutlin treatment (**Figure S3A**, **D**).

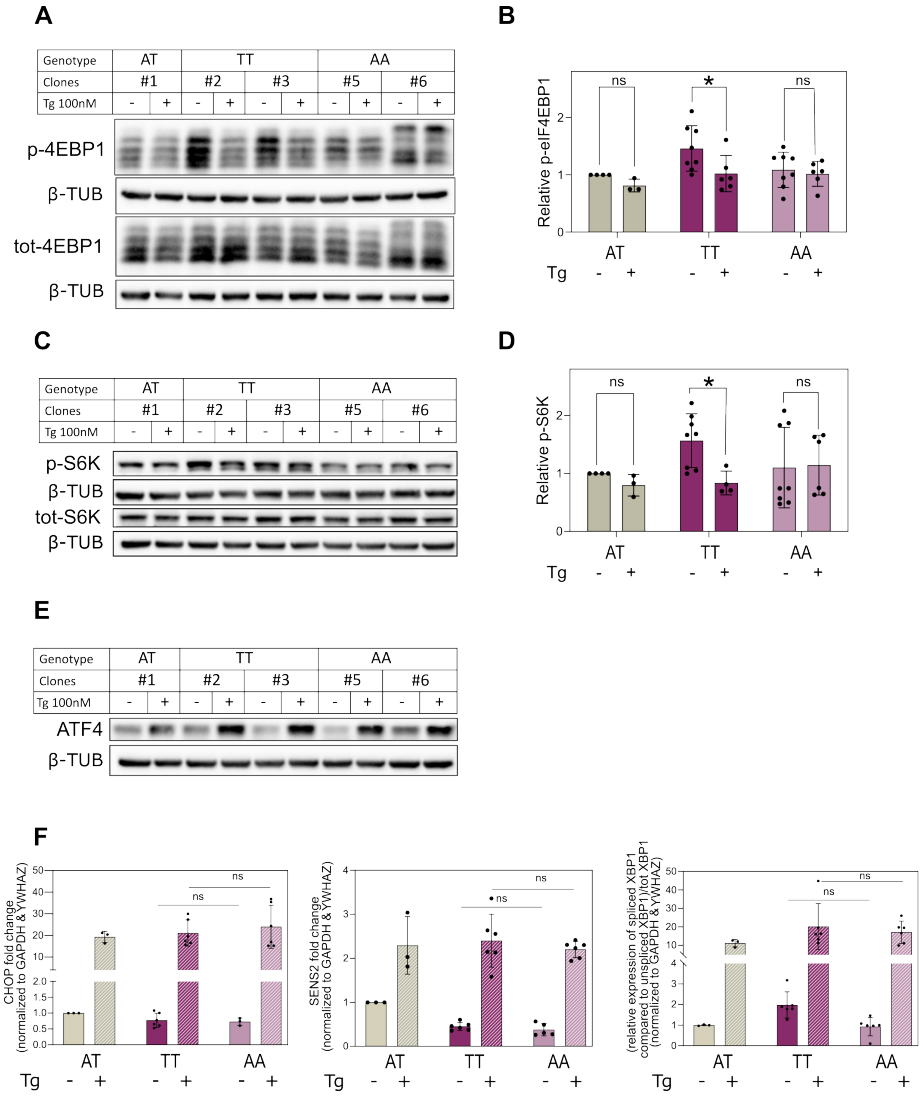

Figure 5. DDIT4 rs1053639 genotype-specific effect on the mTOR pathway.
HCT116 parental cells and clones differing for the rs1053639 homozygous genotypes were treated with either thapsigargin 100nM (Tg) or vehicle control for 4 hours. **A, C**) Cell lysates were analyzed by immunoblotting for the phosphorylation state and levels of the mTORC1 target eIF4EBP1 and S6K proteins. **B, D**) Densitometry analysis of all blots reveals that significant inhibition of the phosphorylation of both eIF4EBP1 and S6K proteins is apparent only in the rs1053639 TT homozygous clones. *p-value <0.05. ns = not significant, unpaired t-test. **E, F**) ER stress response markers are activated in HCT116 cells in response to thapsigargin treatment independently of the rs1053639 genotype. **E)** Western blot analysis of ATF4 protein induction upon thapsigargin (Tg) treatment in HCT116 cells (A/T heterozygous) and DDIT4 rs1053639 homozygous clones (TT, AA). β-Tubulin was used as a reference. F) Relative CHOP, SENS2, and spliced XBP1/unspliced XBP1 mRNA expression as measured by RT-qPCR and normalized to GAPDH and YWHAZ ns = not significant, unpaired t-test.

Next, we investigated whether the differences in the mTOR pathway led to changes in global translation or proliferation of the HCT116 edited clones. The global translation was monitored either in mock culture conditions or in response to Thapsigargin treatment using a quantitative analysis of the Translation Efficiency (TE) measured as the relative abundance of polysomes compared to the 80S from polysomal profiling or the measurement of newly synthesized peptides using either a commercially available global protein synthesis kit or a puromycilation assay (**Figure 6A-C**, **Figure S4A**).

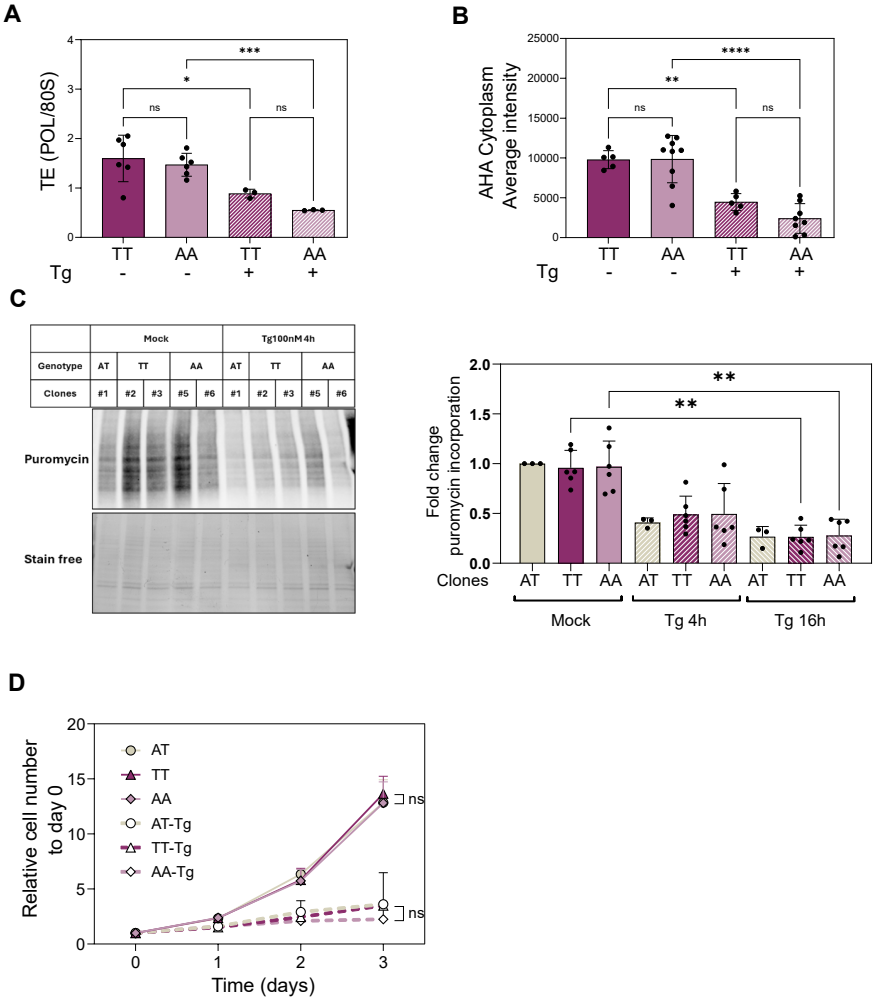

Figure 6. The DDIT4 rs1053639 genotype does not significantly impact global translation and cell proliferation in response to Thapsigargin.

A) Global Translation Efficiency (TE) measured from polysome profiles (see Figure S4) prepared using sucrose gradient fractionation of homozygous TT and AA HCT116 cells treated as in Figure 1A. **B**) Global translation was measured using a Click-it reaction assay after incubation of the cells with modified methionine for 30 minutes. Homozygous TT and AA HCT116 cells grown in mock conditions or treated with 100 nM Thapsigargin for four hours were tested. In both assays, Thapsigargin led to a reduction in global translation. **C**) Global translation measured by a puromycilation assay. A representative Western blot is presented on the left: immunodetection with an antibody targeting puromycin, and the loading control is shown. The bar graph on the right plots the results of the densitometric analysis of the blots plotted as fold change of puromycin

incorporation for the indicated HCT116 clones and treatment conditions. Average, standard deviations, and individual replicates are shown. *P-value < 0.05; **P-value < 0.001; ***P-value < 0.0005. **** P-value < 0.0001, two-tailed, unpaired t-test. **D**) HCT116 cells parental and clones differing for the rs1053639 homozygous genotypes were treated with thapsigargin 10nM of vehicle control for 72 hours. The proliferation of the clones was followed every 24 hours by the Operetta HCS system. Relative cell number curves were plotted as the mean of several replicates ± standard deviation (SD). ns, not significant. Ordinary two-way ANOVA.

In all cases, there were no significant differences in global translation comparing TT and AA rs1053639 clones, although the latter showed a trend for a stronger reduction in the perturbed conditions. The relative proliferation of the clones was similar in the mock condition and in response to thapsigargin (**Figure 6D**), while TT clones showed slightly higher resistance to Nutlin treatment (**Figure S4B**). We concluded that the rs1053639 tranSNP genotype did not show an overt difference in global translation or cell proliferation.

The rs1053639 tranSNP AA genotype shows a competitive growth advantage in prolonged culture conditions.

Given the contribution of DDIT4 in the negative modulation of a critical and intricate metabolic hub such as mTOR (50), we tried to tease out possible differences in cellular phenotypes due to the rs1053639 genotypes through co-culture experiments where cells could experience fluctuations in nutrient availability in the media. To visualize and count the contribution of each genotype to the total co-culture population, derivative GFP or RFP positive clones were obtained with high clonal purity. Cells were seeded in 6-well plates, and relative cell number was measured either at Operetta High Content Screening (HCS) or by FACS, examining the population every four days, up to fifteen days. Results were expressed as relative fitness, as recently described (51) (**Figure 7A**). Interestingly, while the rs1053639 TT cells showed higher fitness at early times, AA cells progressively gained a proliferative advantage. This result was not influenced by the presence or the type of fluorescent marker (**Figure S6A**). Notably, the depletion of RBMX both in TT and AA cells three days prior to the co-culturing reversed the proliferative advantage phenotype of the AA cells (**Figure 7B**). To further explore the significant difference related to rs1053639, cells were sorted seven days after co-culture, and the two rs1053639 genotypes were examined separately. No significant difference in cell

386 cycle distribution was observed (**Figure 7C**). Finally, the co-culture experiment was repeated in the
387 presence of the Q-VD-OPh pan-caspase inhibitor (52). The progressive advantage of the AA
388 genotype was confirmed, suggesting that apoptosis was not involved in this phenotype (**Figure 7D**).
389 Doxorubicin 3µM was included as a control to induce apoptosis (53,54) (**Figure S6C, S6D**).
390
391

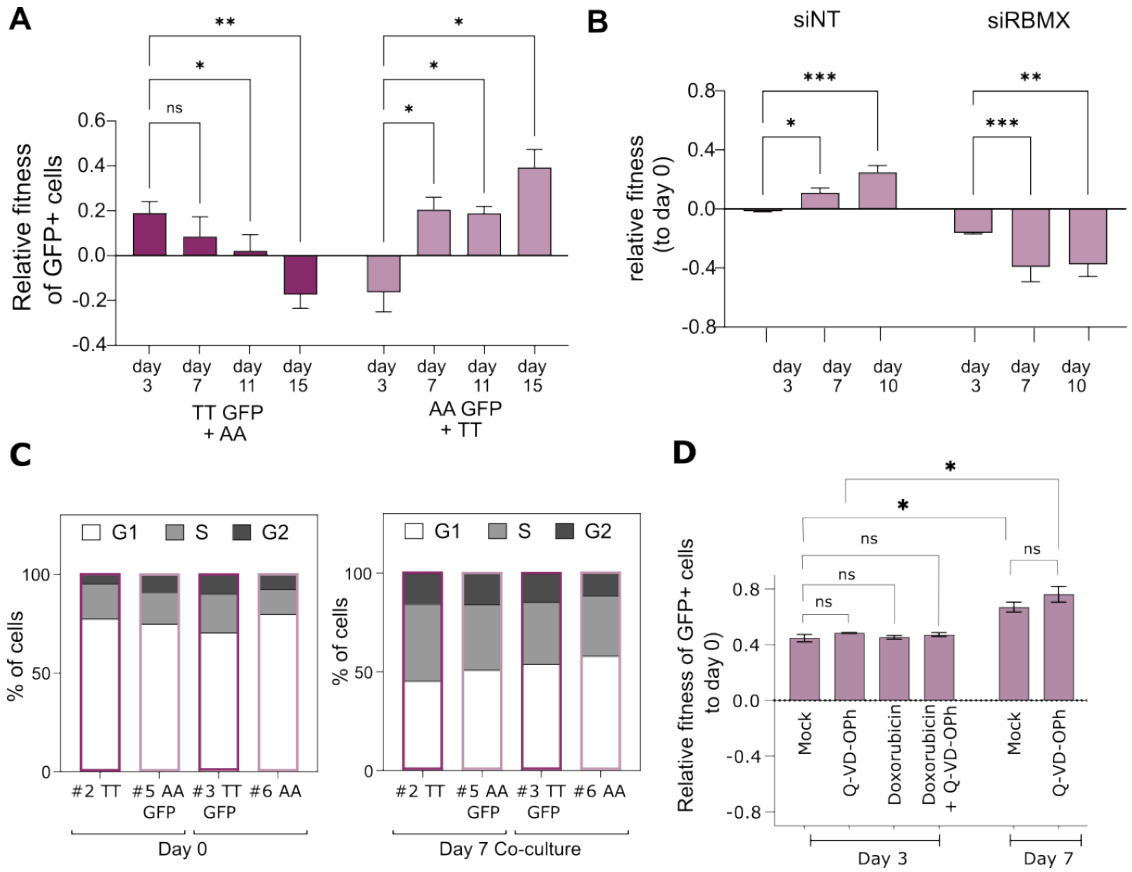

392

393 **Figure 7. DDIT4 rs1053639 impacts cellular dynamics and survival under stress and competitive**
394 **conditions**
395 **A**) DDIT4 clones harboring the TT genotype were transduced with Lentiviral particles to express EGFP
396 constitutively. After transduction, cells were treated with 5 µg/ml blasticidin for at least 15 days, to reach at
397 least 95% of GFP+ cell populations. DDIT4 clones harboring the AA genotype (not fluorescent) were mixed
398 ~1:1 with EGFP-expressing TT genotype cells and co-cultured for 15 days. The relative growth was assessed
399 by flow cytometry, analyzing 10K cells. Cellular fitness of the GFP+ clones relative to GFP- competitor clones
400 was calculated as follows: pGFP+(t) = NGFP+(t) / (NGFP+(t) + N GFP-(t)), W = ln ((pGFP+(ti) /pGFP-(ti))
401 / (pGFP+(t0) /pGFP-(t0)), adapting a described method (51). The error bars represent the mean ± SD of at least
402 eight independent experiments (Four TT GFP+, four AA GFP+). *P-value < 0.05; **P-value <0.01, ordinary
403 two-way ANOVA. **B)** Relative fitness of rs1053639 AA homozygous cells (GFP labeled) in co-culture
404 experiments with the TT homozygous counterpart. Both TT and AA-GFP cells were transfected to deplete
405 RBMX (siRBMX) (or control, siNT) 3 days before starting the co-culture and silenced again at day 3 and day
406 7 during the co-culture experiment. The relative fitness of GFP-positive cells is shown. *P-value < 0.05; **P-
407 value <0.01, ***P-value <0.001, ordinary two-way ANOVA. **C**) Cell cycle analysis by flow cytometry (FACS)
408 for single clones before co-culture (Left) and sorted clones seven days after co-culture (Right). **D**) TT and AA

clones were co-cultured as described in A) up to seven days, in the presence of the pan-caspase inhibitor Q-VD-OPh (10 μM) or vehicle control, and analyzed by FACS at days 0, 3, and 7. As a control, co-cultured cells were treated with Doxorubicin (3μM) +/- Q-VD-OPh (10 μM) for 3 days. The relative fitness of GFP-positive cells across time points and conditions is shown. *P-value < 0.05, two-tailed unpaired t-test.

The rs1053639 tranSNP AA genotype showed faster growth and a competitive advantage when xenografted in Zebrafish embryos.

The proliferation experiments in co-culture suggested to us that the rs1053639 tranSNP genotype could impact cell growth in challenging environments where nutrient concentrations vary, and different cell types can compete. To explore this hypothesis and also gain some information on the potential aggressiveness of our edited cancer cell lines, we developed xenograft experiments in Casper Zebrafish embryos (55), following a published protocol adjusted for our experiments (56). An equal number of cells of the two different genotypes labeled either with GFP or RFP, as described earlier, were injected into the swim bladder of three-day post-fertilization embryos. Cells were then imaged the following day and again 48 hours later. Results, plotted as a percentage of tumor cells' growth comparing 24 to 72 hours post-injection, showed that, when cells of the two genotypes were pre-co-cultured *in vitro* for three days prior to injection in the embryos, the growth advantage of the AA genotype was again apparent (**Figure 8A, B**, **S7A**).

Furthermore, we evaluated the proliferative potential of the TT and AA cells separately in the *in vivo* setting. Notably, the AA cells grew more compared to the TT ones as well (**Figure 8C, D, S7B**). Collectively, co-culture experiments indicate that rs1053639 AA cells display a competitive advantage over TT cells both *in vivo* and *in vitro*, although the underlying mechanisms remain to be clarified, and it does not seem to fit under a classical cell competition response (57).

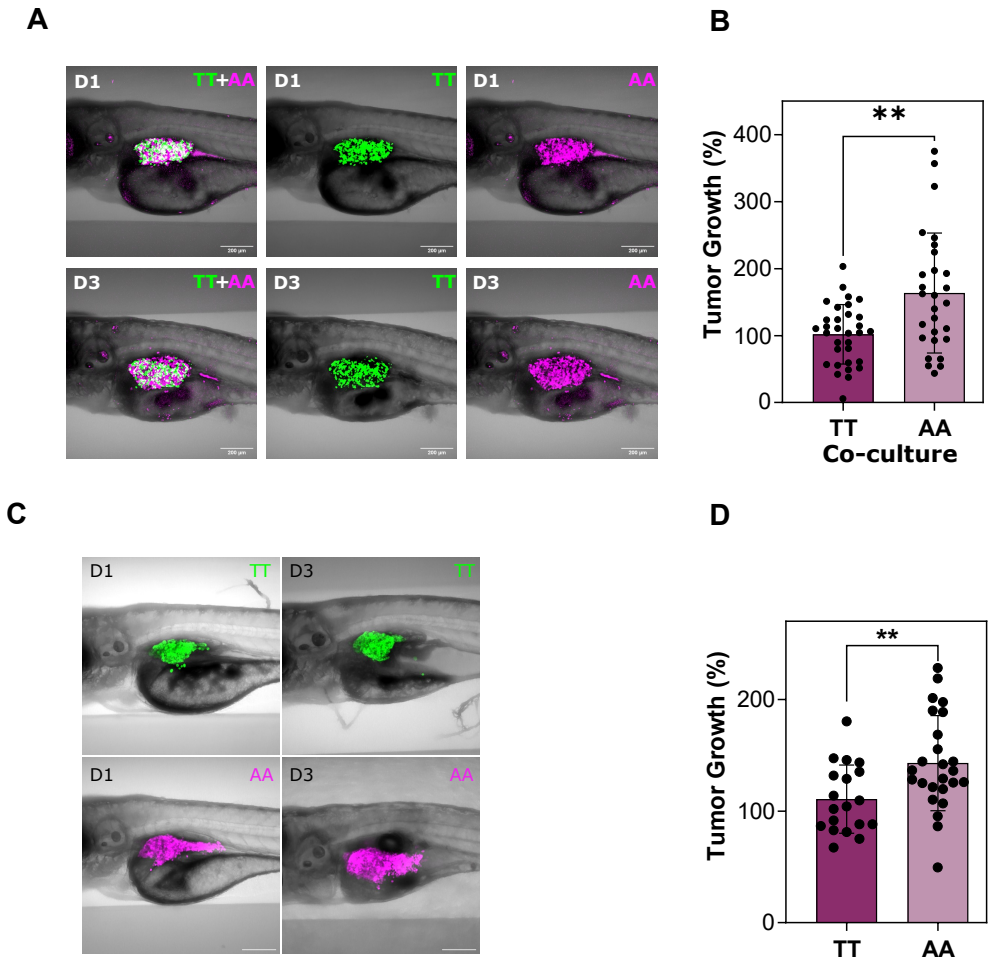

Figure 8. DDIT4 rs1053639 impacts tumor growth and genotypic competition in zebrafish larvae xenotransplants.

DDIT4 rs1053639 homozygous clones, transduced with lentiviral particles to constitutively express either EGFP or MiRFP as described in Figure 5A, were xenotransplanted into zebrafish larvae two days post-fertilization. Tumor growth was monitored over a three-day period, with a minimum of 30 larvae per genotype condition. Representative confocal microscopy images were captured on day 1 and day 3 post-transplantation, with TT clones in green and AA in purple. **A**) DDIT4 clones expressing GFP (TT clones) were mixed~ 1:1 with RFP-expressing clones (AA genotype). They were initially co-cultured *in vitro* for four days, followed by xenotransplantation into ~30 zebrafish larvae for an additional three days of *in vivo* co-growth before confocal imaging. **B**) Bar graph illustrating the percentage of tumor growth relative to day 0 of transplantation, with each data point representing an individual larva. AA clones harbor significantly higher fitness. **P-value < 0.01. paired t-test. **C**) TT and AA clones were separately xenotransplanted into zebrafish larvae, which were followed for three days and imaged by confocal microscopy. **D)** Quantitative analysis of tumor growth indicates a significantly faster growth rate for AA than TT cells *in vivo*. Each data dot represents one larva. **P-value < 0.01. paired t-test.

The rs1053639 tranSNP status can have prognostic significance in cancer patients.

The phenotypic differences related to the rs1053639 genotype, a relatively common SNP in the human population, led us to explore whether this tranSNP status can impact clinically relevant variables in cancer patients. Based on the results obtained with the three genotypes, particularly the

453 reduced control of the mTOR pathway of the AA homozygous cells, we decided to focus on a
454 recessive model, comparing AA homozygous patients with AT plus TT. Using TCGA data we
455 observed worse prognosis for AA patients in both colorectal and esophageal cancers (**Figure S8A,**
456 **S8B**). DDIT4 mRNA expression showed a prognostic value with high expression, which is associated
457 with reduced survival probability in lung adenocarcinoma but higher survival probability in
458 esophageal cancers, according to recent reports (58–60). In colon adenocarcinomas, DDIT4 mRNA
459 expression is significantly higher than healthy tissues (p-value $8.9e^{-21}$) (**Table S8**). Further, data in
460 DepMap indicate a reasonable level of correlation between DDIT4 protein and mRNA levels
461 (Pearson 0.517, linregress p-value $8.82e^{-5}$) (**Figure S8C**). We began exploring the correlation
462 between rs1053639 genotype and DDIT4 protein levels by IHC in seven biopsies of primary
463 colorectal adenocarcinoma and adjacent resected normal tissues. To this aim, DNA from peripheral
464 blood was obtained from the same group of samples, and the DDIT4 SNP status was genotyped
465 (**Figure S8D**). The samples were classified by certified pathologists in two categories based on IHC
466 intensity. The average signal intensity on the different samples, first classified as Low, Intermediate,
467 and High, was re-evaluated using Fiji, and it was found that the average intensity of the Intermediate
468 samples was comparable to the average intensity of the Low samples. Therefore, it was decided to
469 reduce the classes from three to two (Low and High). Overall, cytoplasmic expression of DDIT4
470 protein was higher in the cancer samples than in healthy tissue from the same patient. Only one
471 sample (TT) received a high score both for normal and tumor sections (**Figure S8D**, **E1**, and **E2**).
472 Further studies are needed to establish the value of rs1053639 SNP status as a prognostic marker.
473

474 # Discussion

475 *Variation in allelic imbalance in polysomal RNA as a tool to identify functionally relevant SNPs.*
476 Our approach to identifying tranSNPs is based on computing and comparing relative changes in allele
477 counts across mRNA fractions, building upon the methodology previously introduced (9), and the
478 underlying assumption in our approach is that the interaction of an mRNA with polysomes is directly
479 proportional to the amount of protein being produced (61). By fully leveraging biological replicates,

480 our enhanced method eliminates the need for a predefined threshold to detect allele-specific
481 expression. Instead, it evaluates differential allelic fractions between RNA-seq data from the two
482 distinct cellular compartments using pairwise statistics, thereby improving the robustness of the
483 analysis. Despite the limitations imposed by low coverage, which introduced noise in allelic fraction
484 estimates and constrained our ability to detect and characterize SNPs with significant allelic
485 imbalances, our findings support the presence of signal in over 11% of analyzable genes. Each of
486 these genes harbors one or multiple imbalanced SNPs, collectively accounting for approximately 7%
487 of all analyzable SNPs, aligning with previous reports (8,9).

488 *Mechanism of rs1053639 impact on DDIT4 protein expression.*

489 For rs1053639 A/T we observed a significant reduction in the alternative allele (A) in polysome-
490 associated mRNAs in the mock condition. Using edited HCT116 clones homozygous for the
491 alternative and reference alleles, respectively, we observed a marked difference in DDIT4 protein
492 expression associated with the different SNP status. In our analysis pipeline, we also used predictions
493 of trans factors binding to mRNAs. In this respect, rs1053639 is predicted to affect an RBMX binding
494 motif. Given that RBMX is reported as prevalently nuclear (36), an observation confirmed also for
495 HCT116 cells (**Figure 4C**), we measured DDIT4 mRNA localization comparing the TT and AA
496 homozygous clones. In general, RNA binding proteins binding 3'-UTR sequences can contribute to
497 subcellular mRNA localization and mRNA fate (68). Results indicated higher cytoplasmic
498 localization for the T allele. The transient silencing of RBMX slightly increased the nuclear
499 localization of the T allele and significantly increased the number of perinuclear granules of DDIT4
500 mRNA. This effect was associated with a significant reduction of DDIT4 protein expression with the
501 TT genotype, making it comparable to the levels of the AA clones. In cells of the AA genotype, the
502 number of DDIT4 mRNA perinuclear granules was lower than in TT cells in the mock condition.
503 Interestingly, RBMX depletion did not significantly change the nuclear localization of the DDIT4
504 mRNA A allele, the number of perinuclear granules per cell, or DDIT4 protein levels. The observed
505 increase of perinuclear DDIT4 mRNA granules in the AA clones, irrespective of RBMX expression,
506 and in the TT clones only upon RBMX depletion, suggests an impact of the tranSNP, together with
507 this trans factor, on mRNA export and translation. Indeed, mRNA granules near the nuclear

508 membrane have been considered intermediate sites during mRNA export (69–71). Moreover, recent
509 reports highlighted the relevance of mRNA localization in cytoplasmic compartments for controlling
510 its protein production (68).

511 Collectively, our validation experiments confirmed the observation of allelic imbalance in
512 polysomes and provided evidence that rs1053639 can impact DDIT4 protein expression through a
513 mechanism that comprises mRNA localization, export, modification, and translation efficiency.

514

515 *Implications of rs1053639 allelic status on DDIT4-mediated functions*

516 DDIT4 is an established important negative modulator of the mTOR pathway, acting at the level of
517 mTORC1. Consistently, its gene expression is modulated in response to ER stress, with ATF4 as an
518 important transcription factor. It is also inducible by hypoxia and is considered a p53 target gene,
519 although recent data proposed that the contribution of p53 is indirect, via the transcription factor
520 RFX7 (20). In general, mTOR inhibition is growing in relevance in p53-dependent tumor suppression
521 (72). The negative modulation of mTORC1 by DDIT4 is rather established, although reports differ
522 on the exact mechanism (45,50) and its relative relevance in different cell types (73). DDIT4, as the
523 extended name testifies, is considered a player in the DNA damage response, although also, in this
524 regard, mechanistic details are missing. Overall, DDIT4 function in cancer is considered to be tumor
525 suppressive. For example, a relatively recent screen indicated DDIT4 in a short list of p53 pathway
526 targets with strong tumor suppressive potential. In agreement with the centrality of the mTOR
527 pathway for general cell metabolism, DDIT4 has emerged as an important gene in contexts other than
528 cancer, such as liver disease, neurodegeneration, pulmonary injury, and retinopathy (64,74–76). In
529 fact, post-transcriptional regulation of DDIT4 expression has been the subject of different studies that
530 can bear relevance for understanding the impact of rs1053639. For example, two studies pointed to
531 the important role of an antisense transcript (DDIT4-AS1) corresponding to a large portion of DDIT4
532 3'UTR and of the 3' coding sequence, although with different conclusions on the role of the antisense
533 transcript on the sense one (27,28). rs1053639 is included in the antisense. We checked if the allelic
534 status could somehow impact the amount of spliced DDIT4-AS1. In HCT116, the antisense was
535 expressed at a very low level, and there were no appreciable differences among the edited clones

536 (**Figure 2**), indicating that it does not contribute to the difference in DDIT4 protein expression in our
537 context.

538 In HCT116 cells, our experiments demonstrate that rs1053639 SNP status significantly
539 impacts DDIT4 protein levels. The lower expression of DDIT4 in AA homozygous clones is even
540 more pronounced when the gene transcription is induced by ER stress or by Nutlin. Hence, the
541 tranSNP we identified is predicted to impact p53-dependent and, more in general, stress-dependent
542 modulation of DDIT4 with potentially appreciable consequences on the negative modulation of
543 mTOR, impacting translation control, proliferation, autophagy, and cell survival. Given the complex
544 regulation of the mTOR pathway (77), the impact of DDIT4 is expected to be at least in part
545 influenced by tissue type. In HCT116 cells, higher DDIT4 protein levels in the TT homozygous
546 clones are associated with stronger repression of mTORC1 markers. Despite this, TT and AA clones
547 showed similar proliferation in culture plates. However, in vitro co-culture experiments showed a
548 higher proliferation of AA cells. The two separated populations did not show evidence of cell cycle
549 checkpoint activation or apoptosis induction. Silencing of RBMX, which negatively impacts DDIT4
550 protein levels in TT but not AA homozygous cells, led to a reversal of that proliferation advantage.
551 The results of the xenograft transplantation experiments in Zebrafish embryos were also consistent
552 with higher proliferation of HCT116 cells homozygous for the rs1053639 A allele.

553 In general terms, DDIT4 is considered a tumor suppressor gene. However, gene expression
554 data from TCGA indicate an almost equal number of cancer types where DDIT4 expression is higher
555 in normal tissues than in cancer compared to the opposite trend. Also, in terms of survival analysis,
556 high DDIT4 expression has been associated either with a better or worse prognosis. Although the
557 data is exploratory in nature, we found consistent prognostic predictions when TCGA patients'
558 cohorts were stratified based on DDIT4 mRNA levels or for the rs1053639 genotype for LUAD,
559 ESCA, and COAD.

560 *Study Limitations*

561 The limited coverage of our RNA-seq dataset resulted in a relatively small number of heterozygous
562 SNPs available for analysis. This was further constrained by our conservative approach, which
563 requires the heterozygous state of an mRNA variant, a minimum of twenty reads, and consistency

among four biological replicates of total and polysomal RNA sequencing that are then compared to nominate a tranSNP candidate. This strategy reduces the number of genetic variants that can be analyzed with a chosen cell line but enhances the likelihood of detecting true signals. Validation experiments using orthogonal approaches and reporter assays were limited to four selected candidates of which three showed consistent results across methods. While the heterozygous state is a requirement to start our analysis, the phenotypic impact of a variant is expected to be most pronounced in homozygous states. Therefore, confirming the causal role of a tranSNP on cell phenotypes requires the development of genomically edited, isogenic cell clones differing for SNP status, a time-intensive process that, in our study, was performed only in HCT116 cells.

Conclusions

We have developed a robust pipeline to catalog genetic variants associated with allele-specific changes in mRNA translation, leveraging biallelic mRNAs and polysomal profiling as a proxy for translation efficiency (**Figure 9**).

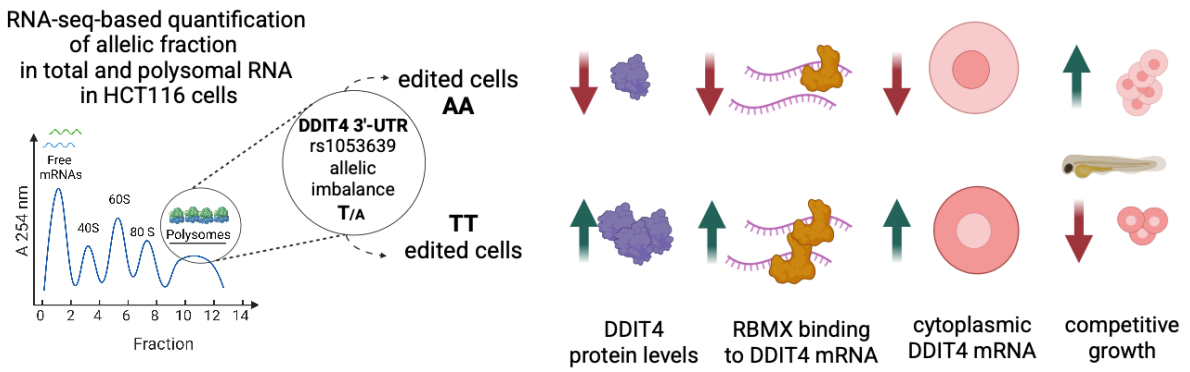

Figure 9. Graphical Summary. Scheme of the approach taken to identify tranSNPs and of the results obtained with rs1053639 in DDIT4 with the HCT116 cell model.

Using this approach, we identified 40 SNPs that exhibit allelic imbalance when comparing total and polysomal RNA. Focusing on rs1053639 in the DDIT4 3'UTR, we found that the alternative (A) allele is associated with reduced DDIT4 protein levels in the human colon adenocarcinoma-derived HCT116 cells. This reduction correlates with a higher abundance of the A allele in the nucleus and

586 an increased number of DDIT4 perinuclear cytoplasmic mRNA granules. These allele-specific
587 differences are mediated by the RNA-binding protein RBMX. Cells homozygous for the alternative
588 A allele exhibit lower DDIT4 protein levels, leading to diminished negative regulation of the
589 mTORC1 pathway, enhanced growth potential in zebrafish xenografts, and poorer prognosis in
590 selected TCGA cancer cohorts. More broadly, our approach provides a powerful framework for
591 identifying genetic drivers of inter-individual variability in mRNA translation, shedding light on
592 mechanisms that can influence cancer progression.
593

594 # Materials and methods

595

596 **Cell lines and cell culturing**

597 The human cell line HCT116 was purchased from the Biological Resource Center ICLC Cell bank.
598 Cells were cultured in standard Roswell Park Memorial Institute (RPMI) 1640 medium (GIBCO)
599 supplemented with 10% fetal bovine serum (FBS), 100 units/ml penicillin, 100 mg/ml streptomycin
600 antibiotic mix (GIBCO), and 2 mM Glutamine (GIBCO). The cells were maintained in a humidified
601 atmosphere at 37°C and 5% CO_2.
602

603 **Dataset and data preprocessing**

604 The RNA-sequencing data of RNA extracted from polled polysomal and total cytoplasmic fractions
605 of HCT116 cells cultured either in mock condition or treated with the MDM2 inhibitor Nutlin was
606 produced in our earlier study (13). The raw data is deposited in GEO, under the GSE95024 accession
607 number. Single-end RNA-seq data was processed to obtain from row FASTQ files properly processed
608 BAM files. The trimming step, essential to remove sequence adapters, was performed with
609 Trimmomatic (78). The data were aligned with STAR (79) to the reference genome GRCh38 to
610 obtain a BAM file for each sample. To improve the characterization of SNP positions, a step of
611 deduplication to remove PCR artifacts was performed by employing PICARD module
612 MarkDuplicates (broadinstitute.github.io/picard/). Then, GATK (80) was employed to split, realign,

613 and recalibrate the data in order to improve the quality of the alignment. The pileup of SNPs positions
614 was performed with ASEQ (81) using parameters mode=0, mbq=20, and mrq=20 in order to obtain
615 allelic fraction (AF) calculations. Only SNPs in exonic and UTR regions extracted from dbSNP were
616 considered. We emphasize that, as expected, the use of single-end RNA-seq data led to high
617 duplication rates (on average 70%), limiting the number of SNPs we could characterize and analyze.
618 Nevertheless, this step, along with subsequent quality control processes, was essential to ensuring
619 high-quality AF estimations.
620 .
621
622 **Differential ASE analysis**
623 The allelic fraction at SNPs' positions was used to compute differential allele-specific expression
624 (ASE) events between total and polysomal RNA fractions. In order to capture those events, we started
625 by identifying all SNPs that were heterozygous in at least one biological replicate of the two fractions.
626 More specifically, to define the analyzable SNPs, for the data obtained both in mock and Nutlin-
627 treatment conditions, we searched for SNPs having a value of AF between 0.2 and 0.8 (i.e.,
628 heterozygous genotype) in at least one replicate of one of the two fractions (polysomal or total) and
629 that were confidently observable, i.e., with a depth of coverage of at least 20x of the SNP site in the
630 each fraction, condition, and biological replicate. A total of 1060 SNP/condition pairs were identified.
631 Of these, only those with AF measures available across all four biological replicates and both
632 fractions were then considered for differential ASE analysis (N=582, Table S1).
633 To assess the presence of a differential ASE event at a SNP position we extended the methodology
634 we developed (9). In particular, for each SNP we exploited the concordance of differential AF
635 measures across pairs of polysomal and total RNA biological replicates by performing paired t-test
636 statistics. Although none of the 41 SNP/condition pairs with nominal p-value ≤ 0.05 kept significance
637 after FDR correction, likely due to the low coverage that increased the noise in AF estimations,
638 overall, 11.8% of the analyzed genes had one or multiple SNPs (in LD) with a p-value ≤ 0.05, strongly
639 supporting the presence of a true signal. A list of SNPs with nominal p-values ≤ 0.05, denoted as
640 putative tranSNPs, were hence retained for downstream analysis and experimental validation.

641

642 **Expression analysis of DDIT4 in cancer and normal tissue samples**

643 To test whether the gene containing the rs1053639 tranSNP exhibits differential expression in tumor
644 versus normal tissue samples, we compared transcript expression values (normalized RPKM values)
645 of the DDIT4 gene exploiting primary tumor and normal tissue samples from the TCGA COAD
646 dataset. In detail, we downloaded the gene counts for all genes from the recount 3 database (82), and
647 RPKM values were computed using the function *getRPKM* from the recount 2 R package. Then,
648 protein-coding transcripts were selected, and their RPKM values were normalized across samples
649 using the R limma quantile normalization function. Then, focusing on the DDIT4 gene, the
650 distributions of log2(RPKM+1) values across tumor and normal samples were compared using
651 Wilcoxon's test statistics, and p-values were finally corrected for multiple hypotheses using the FDR
652 method.

653

654 **Survival assay using TCGA data**

655 Genotype and survival data for TCGA patients were collected. Specifically, genotype information
656 for rs1053639 tranSNPs was retrieved from (83), while survival data across different endpoints
657 (Overall Survival, Disease-Specific Survival, Disease-Free Interval, and Progression-Free Interval)
658 was retrieved from (84). A recessive model (AA+AB vs. BB) was built, and for each endpoint, a
659 Kaplan-Meier survival curve was calculated along with summary statistics obtained from a
660 multivariate Cox proportional hazards regression model, where age at diagnosis was included as a
661 covariate. For each endpoint, the analysis was performed across 23 different cancer types, and p-
662 values were corrected for multiple hypothesis testing, retaining only associations with a p-value <
663 0.05 and an FDR < 0.25. Survival analyses were performed using the survival R package.

664

665 **Identification of SNPs disrupting putative RBP consensus motifs**

666 To investigate the RNA protein binding landscape at the rs1053639 tranSNPs locus, we retrieved 552
667 human RNA binding consensus motifs from the RBPDB database (33) and created a FASTA file
668 containing a list of 60bp DNA sequences containing the reference and the alternative bases. Then,

669 TESS software (34) was run to compute RBP consensus motifs scores. A set of log-likelihood-ratio-
670 based scores were computed: the log-odds ratio of the match for the alternative and reference bases
671 (*altScore* and *refScore*), and the maximum possible log-odds ratio for a match for a given RBP
672 consensus motif (*maxScore*). The scores were filtered by keeping only the forward strand analysis.
673 Results were retained only if the score for the reference or the alternative allele was at least 3 and
674 greater than 0.5 when normalized by the *maxScore*.
675
676 **Polysome profiling, RNA extraction, and Sanger sequencing**
677 HCT116 cells were grown in 150 mm dishes to 80% confluence followed by 100 nM Thapsigargin
678 or vehicle treatment for 4 hours. Cells were then incubated for 10 min with 50 µg /ml cycloheximide
679 at 37°C to disrupt the protein synthesis process and halt translation elongation, thereby immobilizing
680 the ribosomes on the mRNAs and preventing ribosome disassembly. Cells were rinsed with ice-cold
681 PBS containing 50 µg /ml cycloheximide and then gently scraped using 600 µl of ice-cold lysis buffer
682 (20 mM Tris-HCl pH 7.5, 100 mM KCl, 5 mM $MgCl_2$, 0.5 % Nonidet P-40, 0.2 U/µl RNasin®
683 Ribonuclease Inhibitor [Promega], cOmplete™, Mini Protease Inhibitor Cocktail 1X [Roche], 100
684 µg /ml cycloheximide) and collected in an Eppendorf tube. The cells were then incubated on ice for
685 10 min and centrifuged for 10 min at 12,000 *x g* at 4 °C to remove the nuclei. The cytoplasmic lysate
686 was then separated by ultracentrifugation in a Beckman SW41 rotor at 40.000 rpm for 1 hour and 40
687 minutes at 4°C after being loaded onto a 15-50% linear sucrose gradient dissolved in salt buffer (100
688 mM NaCl, 20 mM Tris-HCl pH7.5, and 5 mM MgCl2). The sucrose gradients were fractionated, and
689 the absorbance was measured at 254 nm by the Teledyne Isco model 160 gradient analyzer equipped
690 with a UA-6 UV/VIS detector. Based on density separation, polysomes were isolated from the
691 fractions, and RNA was harvested from these polysomes with the TRIzol® reagent (Invitrogen ™)
692 following the manufacturer's protocol. The RNA was then retro-transcribed, and the sequences
693 containing the candidate TranSNPs were amplified by PCR using AmpliTaq Gold 360 Master Mix
694 (ThermoFisher Scientific) and specific primers (**Table S4**). The PCR products were purified by the
695 spinNAker GEL&PCR DNA purification kit (Euroclone) and subjected to Sanger sequencing by
696 Mix2Seq Kit (Eurofins Genomics) following the manufacturer's protocol. Total RNA was also

697 harvested in parallel for Sanger sequencing. Analysis of the electropherograms was performed by
698 Fiji software. Quantification was performed by assessing the area under the peaks of the tranSNP
699 nucleotides as a metric to calculate allelic fraction. The normalization process considered the relative
700 efficiency of the four nucleotides' incorporation during sequencing, using the information of local
701 surroundings. The allelic fraction for targeted genes was determined for at least three independent
702 experiments. Student's t-test was used to calculate the p-value.
703
704 **Targeted RNA sequencing**
705 Targeted RNA-seq libraries were prepared using custom multiplex primers, each containing an ~25-
706 nucleotide (25-nt) gene-specific sequence and either a 33-nt Illumina adaptor (5′-
707 TCGTCGGCAGCGTCAGATGTGTATAAGAGACAG-3′) at the 5′ end of the forward primer or a
708 34-nt Illumina adaptor (5′-GTCTCGTGGGCTCGGAGATGTGTATAAGAGACAG-3′) at the 5′
709 end of the reverse primer. Targeted RNA-seq libraries were prepared from DNase-treated RNA.
710 cDNA was synthesized using a dTVN primer and purified with SPRIselect beads to remove excess
711 primers. Fifty nanograms (50 ng) of cDNA was amplified (first PCR) using gene-specific forward
712 and reverse primers attached to Illumina-specific adapters for cluster generation and sequencing (5′-
713 Illumina Nextera adaptor + sequence-specific forward and reverse primer sequence-3′, see **Table S4**).
714 A five-cycle second PCR was performed using Phusion High-Fidelity DNA Polymerase
715 (ThermoFisher Scientific, Waltham, MA) to incorporate Illumina Nextera primers for sample
716 indexing. After purification with Beckman Ampure XP beads, quantification with Qubit, and quality
717 control using the PerkinElmer LabChip GX, the indexed libraries were pooled, quantified by qPCR
718 using the Roche KAPA Library Quantification Kit (for Illumina platforms), and sequenced on the
719 Illumina MiSeq platform (Illumina, San Diego, CA) using paired-end 250 bp reads with a NANO
720 flowcell and v2 chemistry reagents. Quality control of raw reads was performed using FastQC
721 (https://www.bioinformatics. babraham.ac.uk/projects/fastqc/). Adapter trimming and quality
722 filtering were then conducting with Trimmomatic v0.39 (78) and CutAdapt 4.1 (85) to remove
723 Nextera adapters and primer sequences. The resulting FASTQ files were then aligned to the GRCh38
724 reference genome using STAR v2.7.10b (79), and alignment files were further processed with

725 clipOverlap tool implemented into BamUtil software v1.0.15 (https://genome.sph.
726 umich.edu/wiki/BamUtil:clipOverlap) to trim overlaps between paired reads. Pileup files and variant
727 statistics, including coverage supporting the reference allele, coverage supporting the alternative
728 allele, and the variant allelic fraction, were generated using PacBAM (86).
729
730 **TranSNP 3'UTR cloning**
731 The 3'UTR regions surrounding the candidate TranSNPs were amplified from the HCT116 genomic
732 DNA, using primers containing XbaI and EcoRI restriction sites and resulting in ~500 bp fragments.
733 (**Table S4**). The resulting PCR fragments were cloned immediately downstream of a modified Firefly
734 Luciferase in pGL4.13 [Luc2/SV40] vector (Promega), where a linker sequence adding an EcoR I
735 site (F: 5' cAa**gaattc**atatgcccgggt 3', R: 5' ctagacccgggcatat**gaatt** 3') was inserted at the original Xba
736 I site to facilitate the insertion of fragments in a desired orientation. Correct cloning was confirmed
737 by colony PCR and Sanger sequencing.
738
739 **Plasmid DNA transfection and Luciferase assay**
740 HCT116 cells were seeded into 96-well plates and transiently transfected the empty pGL4.13
741 modified plasmid or those containing the allele-specific 3'UTRs fragments along with the Renilla
742 control luciferase (pRL-SV40) in A 3:1 ratio (60 ng plus 20 ng) using Lipofectamine™ LTX and
743 Plus™ Reagent (ThermoFisher Scientific). After 48 hours, Firefly and Renilla luciferase activities
744 were quantified using a Dual-Luciferase™ Reporter (DLR™) Assay System (Promega). The
745 transfected cells were lysed with 50ul 1X Passive Lysis Buffer for 15 minutes. The lysates were
746 resuspended, and 15ul of the resuspension was transferred to a white 384-well plate. Subsequently,
747 15ul of LAR (Luciferase assay reagent) was added, and the luminescence was read at the Varioskan
748 LUX Microplate reader. Following this, 15ul of the Renilla substrate was added, and the
749 Luminescence was measured again to quantify Renilla luciferase expression. RNA (TRIzol Reagent,
750 Invitrogen) was extracted from the lysates, and the Firefly Luciferase mRNA was quantified by qPCR
751 for additional normalization.
752

753 **CRISPR/Cas9-mediated knock-in**

754 Edited HCT116 clones at the SNP sites were generated exploiting a CRISPR-Cas9 mediated knock-
755 in with the Cas9 delivered as a ribonucleoparticle (RNP), as previously described (22). We designed
756 a single gRNA (**Table S5**) in a position as close as possible to the tranSNP site to cut both alleles and
757 maximize the efficiency of Homology-directed Repair (HDR) (**Figure S2A)**. The same protocol with
758 few modifications (not providing the donor DNA as a template for repair and not inhibiting DNA-
759 PKcs) was used beforehand to test the cutting efficiency of the guide RNA (gRNA). For both
760 protocols, the gRNA was prepared by mixing 1:1 Alt-R® CRISPR-Cas9 crRNA (IDT™) and Alt-
761 R® CRISPR-Cas9 tracrRNA (IDT™). The mixture was heated at 95°C for 5 minutes and let cool
762 down at room temperature for 5 minutes for optimal annealing. 3 µl of gRNA were further incubated
763 with 120 pmol of recombinant Cas9 for 20 minutes at room temperature to generate the
764 ribonucleoprotein (RNP). In parallel, previously seeded HCT116 wild-type cells were harvested by
765 trypsinization, and 2.5 x 10^5 cells per condition were electroporated in the 4D-Nucleofector™ System
766 (Lonza) using the SE Cell Line 4D-Nucleofector™ X Kit S (Lonza) as described in (22). The
767 electroporation mixture combined 20 µl of cell suspension, 1.2 µl of Alt-R® Cas9 Electroporation
768 Enhancer (IDT™), 5 µl of RNP complex, and PBS to a final volume of 30 µl. In addition to these,
769 1.2 µl of Ultramer® DNA Oligonucleotide (100 µM, IDT™) were added in the case of knock-in
770 generation to provide a template donor DNA for HDR. Electroporated cells were recovered from the
771 strip and seeded in a 12-well plate format either untreated or, in the case of knock-in generation,
772 treated with 1 µM of NU7441 DNA-PKcs inhibitor for 48 hours to favor HDR occurrence. The
773 media, both with and without the drug, was changed after 24 hours. The cells were kept in culture up
774 to full recovery and expanded until 2.5 x 10^5 cells could be harvested for DNA extraction and Sanger
775 sequencing. DNA was extracted by adding 20 µl of the QuickExtract™ DNA Extraction Solution
776 (Lucigen) to the cell pellet. After vortexing, the sample was incubated at 65°C for 15 minutes and
777 98°C for 10 minutes. 1 µl of this DNA was used for the PCR amplification using the GoTaq® Green
778 Master Mix (Promega) in 25 µl of reaction. PCR primers (**Table S4**) were specifically designed to
779 produce 300-700 bp long amplicons and to have the SNP of interest asymmetrically located 100-200
780 bp from one or the other end of the amplicon, to have optimal sequencing interpretation. The PCR

781 product was then purified using the MinElute™ PCR Purification Kit (QIAGEN). 75 ng of purified
782 PCR products were sequenced using the Mix2Seq Kit and Sanger sequencing service provided by
783 Eurofins. The TIDE software (Brinkman et al, 2014) was employed to identify and quantify insertions
784 and deletions (indels) in the bulk edited population. The rs1053639 sgRNA presented a cutting
785 efficiency of around 80%. The Synthego ICE software (Synthego Performance Analysis, ICE
786 Analysis. 2019. v3.0) was employed to assess the knock-in efficiency in the edited bulk population.
787 A limiting dilution assay was performed on the knock-in edited bulk population by seeding 1 cell/well
788 in 96-well plate format to eventually obtain clones. The media was changed once a week for 3-4
789 weeks, then potential clones were expanded to 24-well plates, and at the same time, pellets were
790 harvested for DNA extraction and sequencing. The efficiency of clone production was about 1 in 3
791 seeded cells; 85 clones were screened by sequencing.
792
793 **cDNA synthesis and qRT-PCR**
794 RNA was extracted by using the TRIzol® reagent (Invitrogen™) or the NucleoSpin ® RNA kit
795 (Machery-Nagel) based on the downstream applications. RNA purity and quantity were assessed by
796 NanoDrop™ Spectrophotometer (Thermo Fisher Scientific), followed by random primer-mediated
797 reverse transcription using the RevertAid First Strand cDNA Synthesis Kit (Thermo Fisher
798 Scientific) with 1000 ng of RNA as input. The cDNA was diluted 1:8 and 12.5ng -total RNA
799 equivalent- in 10µl reaction were used in the following RT-qPCR analysis with the qPCRBIO
800 SyGreen Mix (PCR Biosystems). All reactions were performed in 384-well plates using the
801 QuantStudio™ 5 Real-Time PCR System (Applied Biosystems®) instrument. Primers were designed
802 using Primer Blast (NCBI) and are listed in **Table S4**. All kits were used following the manufacturer's
803 instructions. All qPCR reactions were performed in triplicate, and Cq values were averaged. The fold
804 change was calculated using *dCt* and normalized to at least two gene references.
805
806 **RNA half-life measurement**
807 3 x 10^5 HCT116 cells from edited clones were seeded in a 6-well plate format. After 24 hours, cells
808 from the first timepoint (t0) well were collected by trypsinization. The cell pellet was resuspended in

809 500 ul of TRIzol® reagent (Invitrogen™) and frozen at -80°C. The media was aspirated from the
810 remaining wells and replaced with 10 ug/ml Actinomycin D in 2 ml of fresh media to achieve RNA
811 polymerase II inhibition. After 20 minutes, 40 minutes, 1 hour, 2 hours and 4 hours from the
812 treatment, cells were pelleted from the corresponding timepoint wells and resuspended in TRIzol®.
813 Once all the pellets were recovered and frozen, they were thawed at room temperature for 15 minutes
814 and RNA was extracted following the TRIzol® manufacturer's instructions. RNA was quantified
815 using the NanoDrop™ Spectrophotometer (Thermo Scientific™) and 1000 ng of timepoint t0 RNA
816 from each HCT116 clone was retro-transcribed using the RevertAid First Strand cDNA Synthesis
817 Kit (Thermo Scientific™) with random hexamers. For timepoints > t0, RNA was retro-transcribed
818 volumetrically to the reference t0 for each clone. The cDNAs were diluted 1:8 and 2 µl in 10 µl of
819 reaction and were used in the following RT-qPCR analysis with the qPCRBIO SyGreen Mix (PCR
820 Biosystems) and the QuantStudio™ 5 Real-Time PCR System (Applied Biosystems®) instrument.
821 Primers are listed in **Table S4**. GAPDH and 18S rRNA levels were also evaluated as stable mRNAs.
822 The mRNA abundance was calculated relative to the start of transcription inhibition (t0) for each
823 HCT116 clone (2^-dCt). The mRNA decay rate was calculated by a nonlinear regression curve fitting
824 using the one-phase decay function (GraphPad Prism version 10).
825
826 **Western blot analysis**
827 1.6 x 10^5 HCT116 cells from edited clones were seeded in a 6-well plate format. When cells reached
828 70 - 80 % confluence, they were treated with 100 nM Thapsigargin or vehicle for 4 hours. Cells were
829 washed with PBS, and total cellular protein was isolated using a RIPA buffer containing protease
830 inhibitor cocktail (cOmplete™, Mini Protease Inhibitor Cocktail, Roche). Lysates prepared for
831 analysis of phosphorylated proteins were supplemented by a phosphatase inhibitor cocktail
832 (Phosphatase Inhibitor Cocktail I, MedChemExpress). After vortexing and incubation at 4°C for 20
833 min, cell lysates were centrifuged at 15000 rpm at 4°C for 15 min, with supernatant collected and
834 stored at -80°C. Prior to western blotting, the lysates were denatured by boiling at 95°C for 10 min
835 in 1x Laemmli Sample Buffer (Bio-Rad). The protein concentration in each sample was determined
836 using Pierce™ BCA Protein Assay Kits (Thermo Fisher Scientific). Equal amounts of protein from

837 each lysate were then subjected to SDS-PAGE and electrophoretically transferred to a nitrocellulose
838 membrane (Cytiva Amersham™ Reinforced Nitrocellulose Blotting Membrane). Each membrane
839 was blocked with 5% dry milk in phosphate-buffer saline and 0.1% Tween-20 (PBST) for 1 h and
840 then incubated with the indicated primary antibodies overnight at 4°C. The membranes were rinsed
841 and incubated with peroxidase-conjugated secondary antibodies for 1 hour at RT. Immunoblotted
842 membranes were developed with ECL™ Select western blot detection reagents (Amersham
843 Biosciences, UK) and imaged on the ChemiDoc™ XRS imaging system (Bio-Rad). Image processing
844 and densitometric quantification of the bands were performed using the Image Lab software. Protein
845 expression was normalized against housekeeping protein, which was an internal control of protein
846 loading. Relative protein expression was then calculated by dividing the normalized intensity of the
847 condition sample by the control. Antibodies used for western blot analysis are listed in **Table S7**. The
848 corresponding anti-mouse and anti-rabbit secondary antibodies were used at 1:10000 dilutions.
849
850 **Protein half-life by cycloheximide chase assay**
851 6 x 10^5 HCT116 cells with the three genotypes were seeded in a 6-well plate format. After 24 hours,
852 cells from the first timepoint (t0) well were collected by trypsinization. The cell pellet was
853 resuspended in 50 µl of RIPA lysis buffer prepared *as in the Western Blot section* and supplemented
854 with 1X protease inhibitors (Roche). In the meantime, the media was aspirated from the remaining
855 wells and replaced with 100 ug/ml of cycloheximide (Cayman Chemical) in 2 ml of fresh media to
856 prevent further protein synthesis. After 10 minutes, 20 minutes, 30 minutes, and 1 hour from the
857 treatment, cells were pelleted from the wells of the corresponding timepoints and resuspended in
858 RIPA buffer 1X as well. Once all the pellets were harvested, proteins were extracted by centrifugation
859 at 15000 rpm for 20 minutes at 4°C, quantified by the Bicinchoninic Acid Assay (Thermo
860 Scientific™ Pierce™ BCA Protein Assay Kit), and Western Blot was performed as described earlier.
861 35 ug of timepoint t0 protein extract from each HCT116 clone was used in Western Blot. For
862 timepoints > t0, the protein amounts were loaded volumetrically to the reference t0, for each clone.
863 DDIT4 and β-Tubulin antibodies were used as primary antibodies. Mouse secondary antibody was
864 used for both the primary antibodies. β-Tubulin was found to be a stable protein and thus was used

865 as a loading control even in this context. Upon normalization of each DDIT4 band intensity to that
866 of the corresponding β-Tubulin, relative protein abundance over time was calculated to the start of
867 translation inhibition (t0) for each HCT116 clone.
868
869 **Global Translation by Click-iT® metabolic labelling of proteins**
870 Global translation was measured by using the Click-iT™ Plus OPP Alexa Fluor™ 488 Protein
871 Synthesis Assay Kit according to the manufacturer's instructions. The fluorescence was measured by
872 the ImageXpress High-Content imaging system (Molecular Devices).
873
874 **Global translation by Puromycin incorporation assay**
875 6 x 10^5 HCT116 cells with the three genotypes were seeded in a 6-well plate format. When the cells
876 reached 60% confluence, they were treated with vehicle or 100nM Thapsigargin for 4 or 16 hours.
877 1μM puromycin was added for 30 min at 37°C prior to pellet collection. Cycloheximide 100 μg/ml
878 was used as a positive control. The cells were lysed, and the puromycin incorporation was assayed
879 by western blot as described above. Stain-free intensity was measured as the reference.
880
881 **Cell proliferation assay**
882 HCT116 DDIT4 edited clones were seeded at 2.5 x 10^3 per well onto 96-well plates and incubated at
883 37°C in standard conditions. The cell number was followed by the high content fluorescent
884 microscope Operetta (PerkinElmer) in digital phase contrast every 24h for 96 h.
885
886 **RNA immunoprecipitation-qPCR (RIP-qPCR)**
887 8 x 10^6 HCT116 cells from edited clones were seeded in 150 mm cell culture dishes (Sarstedt) and
888 harvested after 48 hours by scraping. Cells were lysed in 800 µl of mild lysis buffer (20 mM HEPES
889 pH 7.9, 150 mM NaCl, 1% Triton-X 100, 10% glycerol, 1 mM $MgCl_2$, 1 mM EGTA, 100 U/mL
890 RNasin (Promega), 1X protease inhibitors (Roche)). After 30 minutes of incubation on ice, the lysate
891 was obtained by centrifugation at 15000 rpm, 4°C for 10 minutes. The protein amount was quantified
892 by the Bicinchoninic Acid Assay (Thermo Scientific™ Pierce™ BCA Protein Assay Kit). Meantime,

893 20 µl of Protein A Dynabeads (Invitrogen™) per condition were washed twice with 500 ul of IPP500
894 buffer (20 mM HEPES pH 7.4, 500 mM NaCl, 1.5 mM $MgCl_2$, 0.5 mM DTT, 0.05% NP40) and
895 incubated with either 0.22 µg of anti-RBMX/hnRNP G antibody (#14794, 1:40, Cell Signaling
896 Technology®) or 0.22 µg of anti-Normal Rabbit IgG antibody (#2729, Cell Signaling Technology®)
897 in 100 µl of IPP500 buffer for 1h 30 at room temperature in a rotating wheel. After antibody
898 conjugation, beads were further washed once with 900 µl of IPP500 buffer and twice with 900 µl of
899 IPP150 1x buffer (20 mM HEPES pH 7.4, 150 mM NaCl, 1.5 mM MgCl2, 0.5 mM DTT, 0.05% NP-
900 40) and once with PBS. Nonspecific binding was blocked by incubating the beads with 300 µl of 10
901 mg/ml Bovine Serum Albumin (BSA) for 30 minutes at room temperature in a rotating wheel. Beads
902 were further washed three times with 800 µl of IPP150 1X buffer and incubated with 1 mg of the
903 protein lysate in IPP150 1X buffer and 1x protease inhibitors in a final volume of 400 µl O/N at 4°C
904 in a rotating wheel. Before the incubation with the beads, 10% of lysate in IPP150 1X buffer was
905 isolated as protein input for Western Blot analysis, and 1% was isolated as RNA input for qPCR
906 analysis. After O/N incubation, the flow-through (unbound lysate) was collected for Western Blot
907 analysis, the beads were washed four times with 800 µl of IPP150 1X buffer, and 10% of the last
908 wash was also collected for Western Blot analysis upon elution in LB 1X (Laemmli Sample Buffer,
909 Bio-Rad) heating at 98°C for 10 minutes. Conversely, elution both for RIP samples (beads) and RNA
910 inputs was performed by incubation with 5 µl of >600 U/ml proteinase K solution (Qiagen) and 150
911 ul of Proteinase K buffer (20 mM Tris-HCl pH 7.4, 10 mM $MgCl_2$, 0.2% Tween-20) at 55°C for 30
912 minutes in a lab heat block shaking at 700 rpm. The output RNA is extracted with TRIzol® reagent
913 (Invitrogen) according to the manufacturer's instructions. The total amount of eluted RNA was
914 retrotranscribed using the RevertAid First Strand cDNA Synthesis Kit (Thermo Scientific) and 1 µl
915 of cDNA in 10 µl of reaction was used in the following RT-qPCR analysis with the qPCRBIO
916 SyGreen Mix (PCR Biosystems) and the QuantStudio 5 Real-Time PCR System (Applied
917 Biosystems®) instrument. Primers are listed in Table S4.
918
919 **RNA Electromobility Shift Assay (REMSA)**

920 The interaction between DDIT4 mRNA and RBMX protein was assessed *in vitro* by REMSA. The
921 full-length recombinant RBMX protein was purchased from Origene (TP710403). FAM-labelled
922 fluorescent RNA probes (GAGGGACUGAUUCCU/AGUGGUUGGAA-3'FAM) for the T and A
923 alleles were purchased from Metabion. The binding reaction was set up in 10 µl in the following
924 binding buffer (10 mM HEPES, 50 mM KCl, 1 mM EDTA, 0.05% NP-40, 10% Glycerol, 0.5 mM
925 DTT, pH 11.5). 10 U of RNasin (1 µl) were also added to each reaction and incubated for 30 minutes
926 at RT in the dark. Upon incubation, 1 µl of 6X Orange Dye was added to each reaction to facilitate
927 the visualization of the samples. The binding complex was resolved by running this reaction on a 6%
928 TBE polyacrylamide native (non-denaturing) gel at 80V for 1 hour in TBE 1X at RT. The gel was
929 pre-run in cold TBE 0.5X at 100V for 30 minutes and imaged using the SYBR filter in the
930 ChemiDoc™ XRS imaging system (Bio-Rad).
931
932 **Cell Fractionation**
933 Cell fractionation was performed using a 0.1% Igepal buffer in PBS 1X as in the REAP fractionation
934 protocol, (87) coupled with an RNA extraction protocol (88) to improve the extraction of the RNA
935 from the nuclei. Briefly, HCT116 TT and AA clones were seeded in 10-cm dishes. Once confluent,
936 cells were detached by trypsinization, washed with PBS, and lysed in 900 µl of ice-cold 0.1% Igepal
937 buffer in PBS 1X buffer for 2 minutes; 300 µl of this lysate were removed as whole cell lysate (WCL).
938 The lysate was then fractionated by centrifugation at 12000 rpm for 40s, at RT. 300 µl of the
939 supernatant were isolated as a cytoplasmic fraction (CYTO). The pellet was washed with 1 ml of
940 0.1% Igepal buffer and centrifuged at 12000 rpm for 40s, at RT to obtain the nuclear fraction. 50 µl
941 out of 300 µl were isolated from each fraction for Western Blot analyses upon further lysis by RIPA
942 buffer. The remaining 250 µl were used for TRIzol-based RNA extraction. To implement RNA
943 extraction, the CYTO and NUCLEI fractions were resuspended in 1 ml of TRIzol. Lower volumes
944 of TRIzol did not successfully extract RNA in our conditions. RNA was incubated for 10 minutes in
945 TRIzol at RT, then 10 µl of EDTA 0.5 M were added before incubation at 65C for 5 min, 600 rpm
946 (or until the pellet was completely dissolved). Subsequently, chloroform was added to follow the
947 conventional TRIzol protocol.

948

949 **RBMX Silencing**

950 HCT116 TT and AA cells were transfected with a single or a mixture of two out of three siRNAs
951 targeting RBMX (IDT) at a final concentration of 40 nM for 48 hours (**Table S4**). Control cells were
952 transfected with a non-targeting siRNA (IDT, 51-01-14-04) in the same conditions. INTERFERin
953 (Polyplus) was used as a transfection reagent.

954

955 **Xenograft of HCT116 cells in zebrafish larvae**

956 **Animal rearing:** Zebrafish (*Danio rerio*) strains were raised and maintained in the Model Organism
957 Facility (MOF) at the Department CIBIO, University of Trento under standard conditions (89). The
958 transgenic zebrafish line *Casper* (55) was used to acquire live images in transparent larvae. All
959 zebrafish studies were performed according to European and Italian law, D.Lgs. 26/2014,
960 authorization11/2023-PR to MM. **Larvae preparation:** Embryos were initially maintained at 28 ◦C
961 at a maximum density of 50 embryos per Petri dish in fish water supplemented with 0.0002%
962 methylene blue (Sigma, Burlington, MA, USA) as an antifungal agent. After 24 h, embryos were
963 placed in fish water without methylene blue. **Xenotransplantation of human cancer cell lines:** the
964 protocol of xenotransplantation procedure was adapted from (56,90). GFP or RFP labeled HCT116
965 cells (edited AA, TT, and AT clones) were harvested from a 100 mm Petri dish on the day of
966 xenotransplantation and resuspended in 70 µl of PBS. 0.5 µL of cell suspension containing 200-400
967 cells was transplanted in the swim bladder of 2 dpf zebrafish larvae anesthetized in 0.16 mg/ml
968 PBS/Tricaine (MS-222) under a Nikon SMZ800 stereomicroscope, using a micromanipulator
969 (Marzhouser Wetzkar MM 33 links) and the manual microinjector (CellTram® 4r Air Eppendorf).
970 Transplanted embryos were maintained at 33°C in fish water. Larvae were selected for good
971 transplantation profile using a Leica MZ 10F fluorescence stereomicroscope. **Live-imaging and**
972 **image analysis:** each larval xenograft was imaged one-day post-transplantation (D1) and 3 days post-
973 transplantation (D3) using Leica TCS SP8 laser scanning confocal system (CD7) (Objectives: 10x/1).
974 Images were acquired in z-stack mode with a z-step interval of 7 µm to a range of 170-230 µm

975 depending on the tumor size. The 488/633 nm lasers were used with appropriate filters to acquire
976 green and red fluorescent cancer cells. Image analysis was performed using Fiji software. To study
977 tumor growth of cancer cells *in vivo*, the maximum projection of every image was created, and a
978 threshold was applied for each larva on day 1 (D1) and day 3 (D3) to generate a mask of the tumor
979 area. The area on D3 was normalized to the area of D1 to assess the percentage of tumor growth for
980 each larva.
981
982 **Single-molecule inexpensive RNA fluorescence in situ hybridization**
983 The smiFISH protocol was adapted from (91). Cells were grown on 22 × 22 mm glass coverslips
984 (Prestige) previously stripped with 1 M HCl, sterilized, and stored in 100% ethanol. Cells were fixed
985 in 4% paraformaldehyde (PFA) (Electron Microscopy Science) for 20 min at room temperature and
986 then washed two times with 1× PBS. Permeabilization was performed in 0.5% Triton X-100, 1× PBS
987 for 5 min at room temperature. Once permeabilized, samples were incubated at room temperature in
988 a solution containing 1× SSC and 15% formamide, for 40 min and placed cell-side down on a 50-µl
989 drop of hybridization buffer containing the probe [1× SSC, 15% formamide, bovine serum albumin
990 (BSA) (4.5 mg/ml), 10.6% dextran sulfate, 2 mM Vanadyl Ribonucleoside Complex (VRC), yeast
991 tRNA (0.4 mg/ml), 1 µl of probe mix] in an air-tight hybridization chamber protected from light
992 overnight at 37°C. The probe mix preparation is described in the next paragraph. The following day,
993 coverslips were washed twice with prewarmed 1× SSC solution containing 15% formamide for 30
994 min at 37°C. After that, coverslips were rinsed twice with 1× PBS, cells were stained with DAPI (1
995 ng/µl) (4′,6-diamidino-2-phenylindole) in 1× PBS, for 12 min at room temperature and washed with
996 1× PBS. Samples were mounted on precleaned glass slides using ProLong Diamond Antifade
997 Mountant (Thermo Fisher Scientific). **smiFISH probe preparation:** probe preparation was
998 performed as described by (91). For DDIT4 detection, 3 primary probes targeting the DDIT4
999 sequence were used and prepared as a 20 µM equimolar mixture in milliQ water. Sequences of the
1000 probes are shown in Table S4. Primary probes were mixed with 50 pmol of fluorescently labeled
1001 secondary probes in 1× NEB3 solution [100 mM NaCl, 50 mM tris- HCl (pH 8), 10 mM MgCl2] in
1002 a final volume of 10 µl. Primary probes were annealed with secondary probes in a PCR thermocycler

1003 (85°C for 3 min, 65°C for 3 min, 25°C for 5 min. As described in the previous paragraph, the probe
1004 mix (1 µl) was used for the smiFISH hybridization buffer preparation. **smiFISH combined with IF:**
1005 the smiFISH technique was performed first, using the protocol described in the smiFISH paragraph,
1006 and followed by the immunofluorescence protocol as described hereafter. After the overnight probe
1007 hybridization, cells were washed twice in prewarmed 1× SSC, 15% formamide solution. After two
1008 rinses in 1× PBS, cells were incubated in blocking solution (1× PBS, 2% BSA, 0.1% Triton X-100)
1009 for 3 hours and incubated for 1 hour at room temperature with the primary antibody diluted in
1010 blocking solution. For RBMX detection, we used the antibody in Table S7 at 1:200 dilution. Cells
1011 were then washed five times for 6 min with 1× PBS, 0.1% Triton X-100, and incubated with the
1012 appropriate fluorescent secondary antibody for 1 hour [goat anti-rabbit Alexa Fluor 488 (AF488),
1013 from Thermo Fisher Scientific, catalog no. A-11034, 1:1500 dilution; donkey anti-mouse AF647,
1014 from Thermo Fisher Scientific, catalog no. A-31571, 1:1000 dilution]. After incubation, cells were
1015 washed five times for 6 min with 1× PBS, 0.1% Triton X-100, and stained with DAPI (1 ng/µl) in 1×
1016 PBS for 12 min. After two washes with 1× PBS, coverslips were mounted on glass slides using
1017 ProLong Diamond Antifade Reagent (Thermo Fisher Scientific). **smiFISH/IF image acquisition by**
1018 **confocal microscopy:** images were acquired using a confocal laser scanning Leica TCS SP8 inverted
1019 microscope (Leica Camera AG) with a plan apochromatic 63×/1.40 oil immersion objective and 2×
1020 zoom. Normal photomultipliers (PMTs) were used to detect DDIT4 smiFISH signal, RBMX, b-
1021 tubulin, and DAPI signals. Optimal acquisition parameters, including nanometer range of excitation,
1022 gain, offset, and laser power, were optimized for the visualization of each fluorophore at the
1023 beginning of the acquisition and maintained throughout each experiment. Z stack images were
1024 acquired in each experiment with a 0.3-µm step and 2048 × 2048 pixel size resolution using Leica
1025 Application Suite X (LAS X) imaging software.
1026
1027 **Confocal image analysis**
1028 Images were analyzed using CellProfiler 4.0.7 (Broad Institute, Inc.). Briefly, cell nuclei were
1029 identified as the primary object using the DAPI signal. For each object, the cellular region was
1030 defined by propagating from the nucleus, applying a low segmentation threshold to the smoothed

1031 smiFISH signal. The cytoplasm was defined as a tertiary object by subtracting the nuclear masks
1032 from the cellular regions. DDIT4 smiFISH signal spots were segmented as objects with a typical
1033 diameter range of 10 to 30 pixels. Subsequently, objects were localized based on their position
1034 relative to the nuclear or cytoplasmic regions. Since the majority of the spots exhibited a perinuclear
1035 localization, the nuclear regions were reduced by 5% to prevent misleading classification.
1036 Morphological features and intensity values for both DDIT4 smiFISH and RBMX signals were
1037 calculated at the object level.
1038

1039 **Immunohistochemistry**

1040 Briefly, three-micron sections from paraffin blocks by seven patients with colon adenocarcinoma
1041 were cut and incubated (37°C overnight). IHC staining was performed using Bond III IHC autostainer
1042 for full Automated Immunohistochemistry (Leica Biosystems). Antigens were unmasked with Bond
1043 Epitope Retrieval Solution 1 Leica AR9961 and incubated with the following antibody (diluted with
1044 Bond Primary Antibody Diluent, AR9352 Leica): DDIT4/REDD1 at dilution 1:400 (Proteintech
1045 10638-1-AP). Samples were stained with BOND IHC Polymer Detection Kit (DS9800) and
1046 counterstained using Hematoxylin solution (Leica). The IHC score was obtained by analyzing the
1047 slides by a certified pathologist (G.B.) and applying also ImageJ, a digital image processing software.
1048 Informed consent was obtained from all patients for the use of tissue materials for research purposes.
1049

1050 **Statistical analysis**

1051 Results were plotted and statistically analyzed using GraphPad Prism, version 10. The statistical test
1052 applied, the number of replicates, and the level of significance are provided in each figure legend.
1053

1054 **Declarations**

1055 **Ethics approval and consent to participate**

1056 Informed consent was obtained from all patients for the use of tissue materials for research purposes.

1057 **Availability of data and materials**

1058 The RNA-seq dataset re-analyzed for this study is deposited in GEO under the GSE95024 accession
1059 number.

1060 **Competing interests**

1061 The Authors declare no competing interests

1062 **Authors' contributions**

1063 MHH and LA performed most of the experiments, prepared figures and contributed to the first draft
1064 of the manuscript; TV, SV, DD, performed the RNA-sequencing analysis and developed the pipeline
1065 to identify tranSNPs; FL, performed with MHH and LA the experiments in Zebrafish and prepared
1066 the first draft of the relative methods and results; AM, VV supported the DDIT4 gene editing
1067 approaches; GPG performed with LA the smiFISH experiments; AM supported the design and
1068 execution of the cell sorting experiments; PG, MP supported all HTS-based experiments; CV, VdS,
1069 RB designed the targeted resequencing and performed RNA-sequencing experiments; VM
1070 supervised MHH in planning and performing translation assays; EC contributed to the design and the
1071 evaluation of the results of smiFISH experiments; SF, GB performed, analyzed and interpreted the
1072 IHC data; SZ supervised LA in designing and performing in vitro RBMX-RNA binding and GLORI
1073 at DDIT4 3'UTR; MM supervised and contributed to the design and interpretation of the experiments
1074 in zebrafish; LLF supervised the editing approaches, contributed to the design, visualization and
1075 interpretation of the co-culture experiments, contributed to drafting and revising the manuscript; AR
1076 supervised the study, in particular RNA-seq data analyses, preparation of Tables, drafting of the
1077 manuscript; AI supervised the study, secured the main findings, drafted the manuscript.

1078 **Acknowledgments**

1079 We thank Dr. Ainan Geng and Prof. Hashim M. Al-Hashimi, Department of Biochemistry and
1080 Molecular Biophysics, Columbia University, NYC, USA, for the DDIT4 3'UTR RNA structural
1081 predictions. We thank Dr. Mounira Chalabi, Ribosome, Translation and Cancer Team Universite'
1082 Claude Bernard Lyon, France, for technical support to M.H.H. We thank Alice Casata, Irene Cagol,
1083 Massimo Andreis, Micol Bottamedi, Federica Sontacchi, and Christian Cestaro for technical support
1084 during their Bachelor's internships. We thank Dr. Ezequiel Mariano Rivero and Prof. Fatima
1085 Gebauer, Gene Regulation, Stem Cells, and Cancer Program, Centre for Genomic Regulation (CRG),

Barcelona, Spain, for support with the RIP protocol. We thank Dr. Gabriella Viero, Institute of Biophysics, CNR Unit at Trento, Italy, for support with sucrose gradient fractionation and data analysis.

Funding

This work was supported by Fondazione AIRC under the grant IG #25849 “Mining common genetic variants impacting on allele-specific translation and cancer risk” to A.I, the European Union under NextGenerationEU, PNRR M4C2 INV 1.1, PRIN 2022 PNRR Prot. n. P2022A9J9L to L.L.F. L.A. was supported by an AIRC short-term fellowship. M.C.M. and F.L. were supported by AIRC IG 2021 no. 25704. A.L. and M.H.H. were also supported by Short-term scientific mission fellowships by the “Translation Control in Cancer” European Network”, Translacore Cost Initiative (CA21154). This work was also partially supported by the initiative "*Dipartimenti di Eccellenza* 2023-2027 (Legge 232/2016)" funded by the MUR, and by FESR 2023 – “Sostegno alle Infrastrutture di Ricerca”.

References

1. Xu Y, Ruggero D. The Role of Translation Control in Tumorigenesis and Its Therapeutic Implications. Vol. 4, Annual Review of Cancer Biology. 2020. p. 437–57.
2. Schafer S, Adami E, Heinig M, Rodrigues KEC, Kreuchwig F, Silhavy J, et al. Translational regulation shapes the molecular landscape of complex disease phenotypes. Nat Commun. 2015;6(7200).
3. Fujii K, Shi Z, Zhulyn O, Denans N, Barna M. Pervasive translational regulation of the cell signalling circuitry underlies mammalian development. Nat Commun. 2017;8(14443).
4. Robichaud N, Sonenberg N, Ruggero D, Schneider RJ. Translational control in cancer. Cold Spring Harb Perspect Biol. 2019;11(7).
5. De La Chapelle A. Genetic predisposition to human disease: Allele-specific expression and low-penetrance regulatory loci. Vol. 28, Oncogene. 2009. p. 3345–8.
6. St. Pierre CL, Macias-Velasco JF, Wayhart JP, Yin L, Semenkovich CF, Lawson HA. Genetic, epigenetic, and environmental mechanisms govern allele-specific gene expression. Genome Res. 2022;32(6):1042–57.
7. Lee C, Kang EY, Gandal MJ, Eskin E, Geschwind DH. Profiling allele-specific gene expression in brains from individuals with autism spectrum disorder reveals preferential minor allele usage. Nat Neurosci. 2019;22(9):1521–32.
8. Przytycki PF, Singh M. Differential Allele-Specific Expression Uncovers Breast Cancer Genes Dysregulated by Cis Noncoding Mutations. Cell Syst. 2020;10(2):193-203.e4.
9. Valentini S, Marchioretti C, Bisio A, Rossi A, Zaccara S, Romanel A, et al. TranSNPs: A class of

1120 functional SNPs affecting mRNA translation potential revealed by fraction-based allelic imbalance.
1121 iScience. 2021;24(12).
1122 10. Pringle ES, McCormick C, Cheng Z. Polysome Profiling Analysis of mRNA and Associated Proteins
1123 Engaged in Translation. Curr Protoc Mol Biol. 2019;125(1).
1124 11. Heyer EE, Moore MJ. Redefining the Translational Status of 80S Monosomes. Cell. 2016;164(4):757–
1125 69.
1126 12. Clamer M, Tebaldi T, Lauria F, Bernabò P, Gómez-Biagi RF, Marchioretto M, et al. Active Ribosome
1127 Profiling with RiboLace. Cell Rep. 2018;25(4):1097-1108.e5.
1128 13. Rizzotto D, Zaccara S, Rossi A, Galbraith MD, Andrysik Z, Pandey A, et al. Nutlin-Induced Apoptosis
1129 Is Specified by a Translation Program Regulated by PCBP2 and DHX30. Cell Rep. 2020;30(13):4355-
1130 4369.e6.
1131 14. Marcel V, Van Long FN, Diaz JJ. 40 Years of Research Put P53 in Translation. Vol. 10, Cancers. 2018.
1132 15. Marcel V, Ghayad SE, Belin S, Therizols G, Morel AP, Solano-Gonzàlez E, et al. P53 Acts as a
1133 Safeguard of Translational Control by Regulating Fibrillarin and rRNA Methylation in Cancer. Cancer
1134 Cell [Internet]. 2013;24(3):318–30. Available from: http://www.ncbi.nlm.nih.gov/pubmed/24029231
1135 16. Tiu GC, Kerr CH, Forester CM, Krishnarao PS, Rosenblatt HD, Raj N, et al. A p53-dependent
1136 translational program directs tissue-selective phenotypes in a model of ribosomopathies. Dev Cell.
1137 2021;56(14):2089-2102.e11.
1138 17. Zhang J, Chen X. Posttranscriptional Regulation of p53 and its Targets by RNABinding Proteins. Curr
1139 Mol Med. 2008;8(8):845–9.
1140 18. He X, He L, Hannon GJ. The guardian's little helper: MicroRNAs in the p53 tumor suppressor network.
1141 Cancer Res [Internet]. 2007;67(23):11099–101. Available from:
1142 http://www.ncbi.nlm.nih.gov/entrez/query.fcgi?cmd=Retrieve&db=PubMed&dopt=Citation&list_uid
1143 s=18056431
1144 19. Marcel V, Catez F, Diaz JJ. P53, a translational regulator: Contribution to its tumour-suppressor
1145 activity. Oncogene [Internet]. 2015;34(44):5513–23. Available from:
1146 http://www.ncbi.nlm.nih.gov/pubmed/25728674
1147 20. Coronel L, Häckes D, Schwab K, Riege K, Hoffmann S, Fischer M. p53-mediated AKT and mTOR
1148 inhibition requires RFX7 and DDIT4 and depends on nutrient abundance. Oncogene. 2022;41(7):1063–
1149 9.
1150 21. Sofer A, Lei K, Johannessen CM, Ellisen LW. Regulation of mTOR and Cell Growth in Response to
1151 Energy Stress by REDD1. Mol Cell Biol. 2005;25(14):5834–45.
1152 22. Ghetti S, Burigotto M, Mattivi A, Magnani G, Casini A, Bianchi A, et al. CRISPR/Cas9
1153 ribonucleoprotein-mediated knockin generation in hTERT-RPE1 cells. STAR Protoc. 2021;2(2).
1154 23. Schupp M, Chen F, Briggs ER, Rao S, Pelzmann HJ, Pessentheiner AR, et al. Metabolite and
1155 transcriptome analysis during fasting suggest a role for the p53-Ddit4 axis in major metabolic tissues.
1156 BMC Genomics. 2013;14(1).
1157 24. Ellisen LW, Ramsayer KD, Johannessen CM, Yang A, Beppu H, Minda K, et al. REDD1, a
1158 developmentally regulated transcriptional target of p63 and p53, links p63 to regulation of reactive
1159 oxygen species. Mol Cell. 2002;10(5):995–1005.
1160 25. Brinkman EK, van Steensel B. Rapid Quantitative Evaluation of CRISPR Genome Editing by TIDE

1161 and TIDER. In: Methods in Molecular Biology. Humana Press Inc.; 2019. p. 29–44.
1162 26. Conant D, Hsiau T, Rossi N, Oki J, Maures T, Waite K, et al. Inference of CRISPR Edits from Sanger
1163 Trace Data. Cris J. 2022;5(1):123–30.
1164 27. Yang B, Xu B, Yang R, Fu J, Li L, Huo D, et al. Long Non-coding Antisense RNA DDIT4-AS1
1165 Regulates Meningitic Escherichia coli-Induced Neuroinflammation by Promoting DDIT4 mRNA
1166 Stability. Mol Neurobiol. 2022;59(3):1351–65.
1167 28. Fang Y, Wu X, Gu Y, Shi R, Yu T, Pan Y, et al. LINC00659 cooperated with ALKBH5 to accelerate
1168 gastric cancer progression by stabilising JAK1 mRNA in an m 6 A-YTHDF2-dependent manner . Clin
1169 Transl Med. 2023;13(3).
1170 29. Kimball SR, Jefferson LS. Induction of REDD1 gene expression in the liver in response to endoplasmic
1171 reticulum stress is mediated through a PERK, eIF2α phosphorylation, ATF4-dependent cascade.
1172 Biochem Biophys Res Commun. 2012;427(3):485–9.
1173 30. Protiva P, Hopkins ME, Baggett S, Yang H, Lipkin M, Holt PR, et al. Growth inhibition of colon cancer
1174 cells by polyisoprenylated benzophenones is associated with induction of the endoplasmic reticulum
1175 response. Int J Cancer. 2008;123(3):687–94.
1176 31. Sagara Y, Fernandez-Belda F, De Meis L, Inesi G. Characterization of the inhibition of intracellular
1177 Ca2+ transport ATPases by thapsigargin. J Biol Chem. 1992;267(18):12606–13.
1178 32. Panda A, Martindale J, Gorospe M. Polysome Fractionation to Analyze mRNA Distribution Profiles.
1179 Bio-Protocol. 2017;7(3):e2126.
1180 33. Cook KB, Kazan H, Zuberi K, Morris Q, Hughes TR. RBPDB: A database of RNA-binding
1181 specificities. Nucleic Acids Res. 2011;39(SUPPL. 1):D301-8.
1182 34. Schug J. Using TESS to predict transcription factor binding sites in DNA sequence. Current Protocols
1183 in Bioinformatics. 2008. p. unit 2.6.
1184 35. Liu N, Zhou KI, Parisien M, Dai Q, Diatchenko L, Pan T. N6-methyladenosine alters RNA structure
1185 to regulate binding of a low-complexity protein. Nucleic Acids Res. 2017;45(10):6051–63.
1186 36. Heinrich B, Zhang Z, Raitskin O, Hiller M, Benderska N, Hartmann AM, et al. Heterogeneous nuclear
1187 ribonucleoprotein G regulates splice site selection by binding to CC(A/C)-rich regionsin pre-mRNA. J
1188 Biol Chem. 2009;284(21):14303–15.
1189 37. Zuccotti P, Peroni D, Potrich V, Quattrone A, Dassi E. Hyperconserved Elements in Human 5′UTRs
1190 Shape Essential Post-transcriptional Regulatory Networks. Front Mol Biosci. 2020;7.
1191 38. Liu J, Zheng T, Chen D, Huang J, Zhao Y, Ma W, et al. RBMX involves in telomere stability
1192 maintenance by regulating TERRA expression. PLoS Genet. 2023;19(9 September).
1193 39. Dassi E, Zuccotti P, Leo S, Provenzani A, Assfalg M, D'Onofrio M, et al. Hyper conserved elements
1194 in vertebrate mRNA 3'-UTRs reveal a translational network of RNA-binding proteins controlled by
1195 HuR. Nucleic Acids Res [Internet]. 2013/02/05. 2013;41(5):3201–16. Available from:
1196 http://www.ncbi.nlm.nih.gov/pubmed/23376935
1197 40. Sato K, Akiyama M, Sakakibara Y. RNA secondary structure prediction using deep learning with
1198 thermodynamic integration. Nat Commun. 2021;12(1).
1199 41. Fu L, Cao Y, Wu J, Peng Q, Nie Q, Xie X. UFold: Fast and accurate RNA secondary structure
1200 prediction with deep learning. Nucleic Acids Res. 2022;50(3):E14.
1201 42. Lorenz R, Bernhart SH, Höner zu Siederdissen C, Tafer H, Flamm C, Stadler PF, et al. ViennaRNA

Package 2.0. Algorithms Mol Biol. 2011;6(1).
43. Wayment-Steele HK, Kladwang W, Strom AI, Lee J, Treuille A, Becka A, et al. RNA secondary structure packages evaluated and improved by high-throughput experiments. Nat Methods. 2022;19(10):1234–42.
44. Brugarolas J, Lei K, Hurley RL, Manning BD, Reiling JH, Hafen E, et al. Regulation of mTOR function in response to hypoxia by REDD1 and the TSC1/TSC2 tumor suppressor complex. Genes Dev. 2004;18(23):2893–904.
45. Deyoung MP, Horak P, Sofer A, Sgroi D, Ellisen LW. Hypoxia regulates TSC1/2-mTOR signaling and tumor suppression through REDD1-mediated 14-3-3 shuttling. Genes Dev. 2008;22(2):239–51.
46. Leprivier G, Rotblat B. How does mTOR sense glucose starvation? AMPK is the usual suspect. Cell Death Discov. 2020;6(1).
47. Sengupta S, Peterson TR, Sabatini DM. Regulation of the mTOR Complex 1 Pathway by Nutrients, Growth Factors, and Stress. Vol. 40, Molecular Cell. 2010. p. 310–22.
48. Whitney ML, Jefferson LS, Kimball SR. ATF4 is necessary and sufficient for ER stress-induced upregulation of REDD1 expression. Biochem Biophys Res Commun. 2009;379(2):451–5.
49. Han S, Zhu L, Zhu Y, Meng Y, Li J, Song P, et al. Targeting ATF4-dependent pro-survival autophagy to synergize glutaminolysis inhibition. Theranostics. 2021;11(17):8464–79.
50. Dennis MD, Coleman CS, Berg A, Jefferson LS, Kimball SR. REDD1 enhances protein phosphatase 2A-mediated dephosphorylation of Akt to repress mTORC1 signaling. Sci Signal. 2014;7(335).
51. Dias Louro MA, Peneda C, Bank C, Bettencourt-Dias M. Adaptation of human cell populations to different levels of centriole amplification involves a two-step response. bioRxiv [Internet]. 2024;2024.02.15.580424. Available from: http://biorxiv.org/content/early/2024/02/17/2024.02.15.580424.abstract
52. Keoni CLI, Brown TL. Inhibition of apoptosis and efficacy of pan caspase inhibitor, Q-VD-OPh, in models of human disease. Vol. 8, Journal of Cell Death. 2015. p. 1–7.
53. Wang S, Konorev EA, Kotamraju S, Joseph J, Kalivendi S, Kalyanaraman B. Doxorubicin induces apoptosis in normal and tumor cells via distinctly different mechanisms: Intermediacy of H2O2- and p53-dependent pathways. J Biol Chem. 2004;279(24):25535–43.
54. Hamadou MH, Kerkatou M, Gatto P, Pancher M, Bisio A, Inga A, et al. Apigenin rich-Limonium duriusculum (de Girard) Kuntze promotes apoptosis in HCT116 cancer cells. Nat Prod Res. 2021;35(17):2910–4.
55. White RM, Sessa A, Burke C, Bowman T, LeBlanc J, Ceol C, et al. Transparent Adult Zebrafish as a Tool for In Vivo Transplantation Analysis. Cell Stem Cell. 2008;2(2):183–9.
56. Marines J, Lorenzini F, Kissa K, Fontenille L. Modelling 3D Tumour Microenvironment In Vivo: A Tool to Predict Cancer Fate. Curr Issues Mol Biol. 2023;45(11):9076–83.
57. Bowling S, Di Gregorio A, Sancho M, Pozzi S, Aarts M, Signore M, et al. P53 and mTOR signalling determine fitness selection through cell competition during early mouse embryonic development. Nat Commun. 2018;9(1).
58. Song L, Chen Z, Zhang M, Zhang M, Lu X, Li C, et al. DDIT4 overexpression associates with poor prognosis in lung adenocarcinoma. J Cancer. 2021;12(21):6422–8.
59. Fattahi F, Saeednejad Zanjani L, Habibi Shams Z, Kiani J, Mehrazma M, Najafi M, et al. High

1243 expression of DNA damage-inducible transcript 4 (DDIT4) is associated with advanced pathological
1244 features in the patients with colorectal cancer. Sci Rep. 2021;11(1).
1245 60. Chen X, Li Z, Liang M, Zhang Z, Zhu D, Lin B, et al. Identification of DDIT4 as a potential prognostic
1246 marker associated with chemotherapeutic and immunotherapeutic response in triple-negative breast
1247 cancer. World J Surg Oncol. 2023;21(1).
1248 61. Wang ZY, Leushkin E, Liechti A, Ovchinnikova S, Mößinger K, Brüning T, et al. Transcriptome and
1249 translatome co-evolution in mammals. Nature. 2020 Dec 24;588(7839):642–7.
1250 62. Gandin V, Sikström K, Alain T, Morita M, McLaughlan S, Larsson O, et al. Polysome fractionation
1251 and analysis of mammalian translatomes on a genome-wide scale. J Vis Exp. 2014;(87).
1252 63. Liang S, Bellato HM, Lorent J, Lupinacci FCS, Oertlin C, van Hoef V, et al. Polysome-profiling in
1253 small tissue samples. Nucleic Acids Res. 2018;46(1):E3.
1254 64. Qin Y, Li B, Arumugam S, Lu Q, Mankash SM, Li J, et al. m6A mRNA methylation-directed myeloid
1255 cell activation controls progression of NAFLD and obesity. Cell Rep. 2021;37(6).
1256 65. Zhou Y, Zeng P, Li YH, Zhang Z, Cui Q. SRAMP: Prediction of mammalian N6-methyladenosine
1257 (m6A) sites based on sequence-derived features. Nucleic Acids Res. 2016;44(10).
1258 66. Yang X, Liu QL, Xu W, Zhang YC, Yang Y, Ju LF, et al. m6A promotes R-loop formation to facilitate
1259 transcription termination. Vol. 29, Cell Research. 2019. p. 1035–8.
1260 67. Liu C, Sun H, Yi Y, Shen W, Li K, Xiao Y, et al. Absolute quantification of single-base m6A
1261 methylation in the mammalian transcriptome using GLORI. Nat Biotechnol. 2023;41(3):355–66.
1262 68. Horste EL, Fansler MM, Cai T, Chen X, Mitschka S, Zhen G, et al. Subcytoplasmic location of
1263 translation controls protein output. Mol Cell. 2023;83(24):4509-4523.e11.
1264 69. Basyuk E, Rage F, Bertrand E. RNA transport from transcription to localized translation: a single
1265 molecule perspective. Vol. 18, RNA Biology. 2021.
1266 70. Sheth U, Pitt J, Dennis S, Priess JR. Perinuclear P granules are the principal sites of mRNA export in
1267 adult C. elegans germ cells. Development. 2010;137(8):1305–14.
1268 71. Meia M, Cupic A, Miorinb L, Yee C, Cagatay T, Zhangf K, et al. Inhibition of mRNA nuclear export
1269 promotes SARS-CoV-2 pathogenesis. Proc Natl Acad Sci U S A. 2024;121(22):e2314166121_.
1270 72. Kon N, Ou Y, Wang SJ, Li H, Rustgi AK, Gu W. mTOR inhibition acts as an unexpected checkpoint
1271 in p53-mediated tumor suppression. Genes Dev. 2021;35(1):59–64.
1272 73. Chen R, Wang B, Chen L, Cai D, Li B, Chen C, et al. DNA damage-inducible transcript 4 (DDIT4)
1273 mediates methamphetamine-induced autophagy and apoptosis through mTOR signaling pathway in
1274 cardiomyocytes. Toxicol Appl Pharmacol. 2016;295:1–11.
1275 74. Rittenhouse KD, Johnson TR, Vicini P, Hirakawa B, Kalabat D, Yang AH, et al. RTP801 gene
1276 expression is differentially upregulated in retinopathy and is silenced by PF-04523655, a 19-mer siRNA
1277 directed against RTP801. Investig Ophthalmol Vis Sci. 2013;55(3):1232–40.
1278 75. Malagelada C, Ryu EJ, Biswas SC, Jackson-Lewis V, Greene LA. RTP801 is elevated in Parkinson
1279 brain substantia nigral neurons and mediates death in cellular models of Parkinson's disease by a
1280 mechanism involving mammalian target of rapamycin inactivation. J Neurosci. 2006;26(39):9996–
1281 10005.
1282 76. Yoshida T, Mett I, Bhunia AK, Bowman J, Perez M, Zhang L, et al. Rtp801, a suppressor of mTOR
1283 signaling, is an essential mediator of cigarette smoke-induced pulmonary injury and emphysema. Nat

Med. 2010;16(7):767–73.
77. Goul C, Peruzzo R, Zoncu R. The molecular basis of nutrient sensing and signalling by mTORC1 in metabolism regulation and disease. Vol. 24, Nature Reviews Molecular Cell Biology. 2023. p. 857–75.
78. Bolger AM, Lohse M, Usadel B. Trimmomatic: A flexible trimmer for Illumina sequence data. Bioinformatics [Internet]. 2014;30(15):2114–20. Available from: http://www.ncbi.nlm.nih.gov/pubmed/24695404
79. Dobin A, Davis CA, Schlesinger F, Drenkow J, Zaleski C, Jha S, et al. STAR: Ultrafast universal RNA-seq aligner. Bioinformatics. 2013;29(1):15–21.
80. Depristo MA, Banks E, Poplin R, Garimella K V., Maguire JR, Hartl C, et al. A framework for variation discovery and genotyping using next-generation DNA sequencing data. Nat Genet. 2011;43(5):491–501.
81. Romanel A, Lago S, Prandi D, Sboner A, Demichelis F. ASEQ: Fast allele-specific studies from next-generation sequencing data. BMC Med Genomics. 2015 Mar 1;8(1).
82. Wilks C, Zheng SC, Chen FY, Charles R, Solomon B, Ling JP, et al. recount3: summaries and queries for large-scale RNA-seq expression and splicing. Genome Biol. 2021;22(1).
83. Valentini S, Gandolfi F, Carolo M, Dalfovo D, Pozza L, Romanel A. Polympact: Exploring functional relations among common human genetic variants. Nucleic Acids Res. 2022;50(3):1335–50.
84. Liu J, Lichtenberg T, Hoadley KA, Poisson LM, Lazar AJ, Cherniack AD, et al. An Integrated TCGA Pan-Cancer Clinical Data Resource to Drive High-Quality Survival Outcome Analytics. Cell. 2018;173(2):400-416.e11.
85. Martin M. Cutadapt removes adapter sequences from high-throughput sequencing reads. EMBnet.journal. 2011;17(1):10.
86. Valentini S, Fedrizzi T, Demichelis F, Romanel A. PaCBAM: Fast and scalable processing of whole exome and targeted sequencing data. BMC Genomics. 2019;20(1).
87. Suzuki K, Bose P, Leong-Quong RY, Fujita DJ, Riabowol K. REAP: A two minute cell fractionation method. BMC Res Notes. 2010;3.
88. Gagnon KT, Li L, Janowski BA, Corey DR. Analysis of nuclear RNA interference in human cells by subcellular fractionation and Argonaute loading. Vol. 9, Nature Protocols. 2014. p. 2045–60.
89. Kimmel CB, Ballard WW, Kimmel SR, Ullmann B, Schilling TF. Stages of embryonic development of the zebrafish. Dev Dyn. 1995;203(3):253–310.
90. Lorenzini F, Marines J, Friec J Le, Khoa N Do, Nieto MA, Sanchez-Laorden B, et al. Melanoma innervation is associated with cancer progression in a zebrafish xenograft model. bioRxiv [Internet]. 2023;doi:10.110:2023.12.13.571512.Available from: https://www.biorxiv.org/content/10.1101/2023.12.13.571512v1%0Ahttps:// www.biorxiv.org/content/10.1101/2023.12.13.571512v1.abstract
91. Querido E, Sfeir A, Chartrand P. Imaging of Telomerase RNA by Single-Molecule Inexpensive FISH Combined with Immunofluorescence. STAR Protoc. 2020;1(2).

A *TranSNP* in the DDIT4 mRNA can impact its translation efficiency and modulate p53-dependent responses in cancer cells

Meriem Hadjer Hamadou*[1], Laura Alunno*[1] et. al.,

Supplementary Figures and Tables

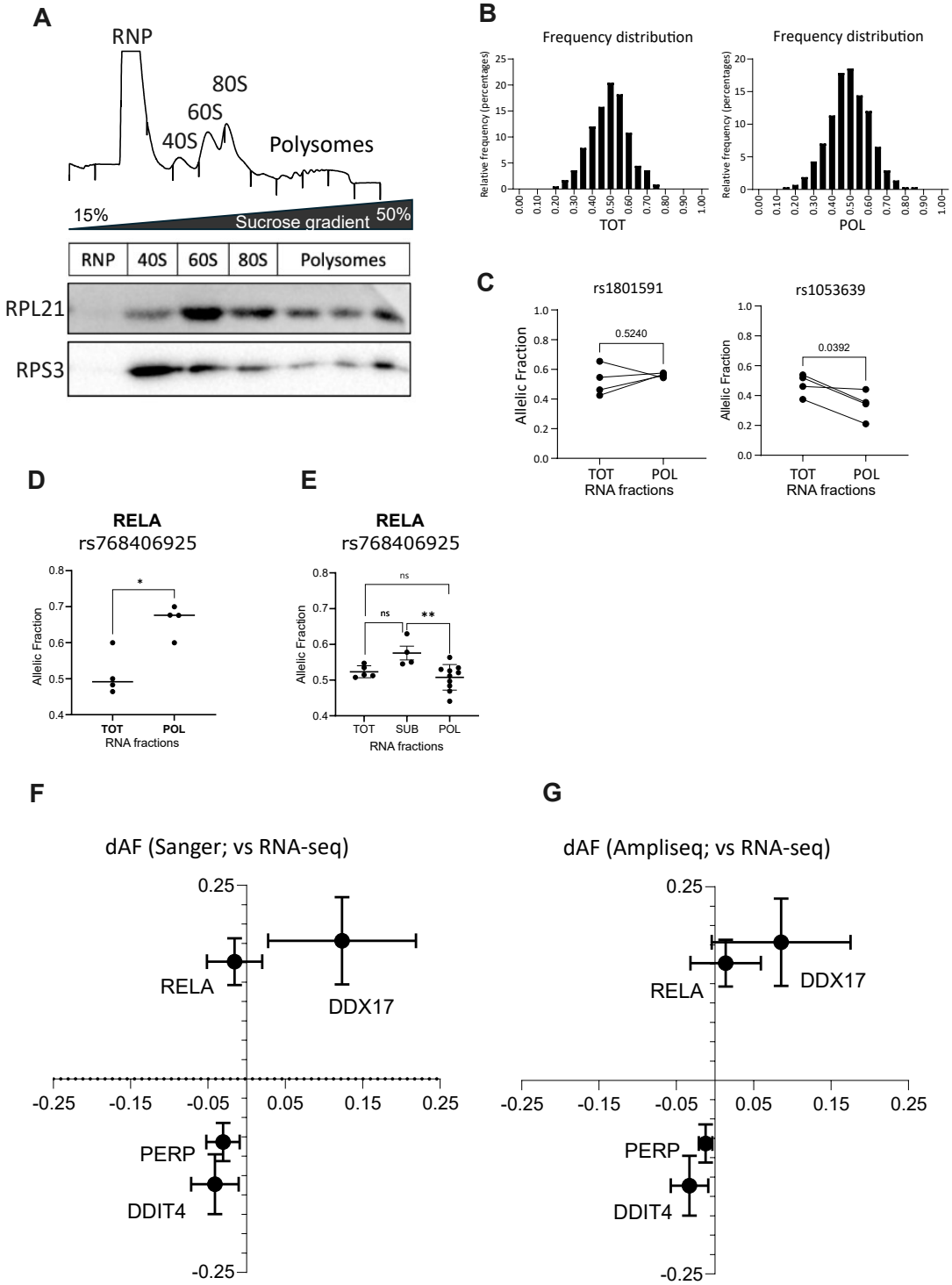

Figure S1. TranSNPs identification and validation -related to Figure 1-.

A) Representative polysome profile of HCT116 cells and western blot results for markers of the small (RPS3) and large (RPL21) ribosomal subunits used as controls for sedimentation. Lysates separated to equilibrium density by

ultracentrifugation on a linear 15-50% sucrose gradient were fractionated following UV absorbance recorded at 254 nm. The fractions representing polysomes (POL) that were pooled together for subsequent analysis are indicated. **B**) Distribution plotted as the percentage of the relative frequency of average allelic fractions for all the heterozygous SNPs that could be studied in the RNA-seq experiment, for total (left figure) and polysomal (right figure) RNA. AF data for each of the four experimental replicates is provided in Table S1. The RNA-seq dataset is deposited in GEO (accession number: GSE95024). **B**) Examples of paired t-test statistics exploited to assess the concordance of differential AF measures across pairs of polysomal and total RNA biological replicates. **D**) Plots of the allelic fraction (the number of alternative allele reads divided by the sum of alternative and reference allele reads) measured for rs768406925 in the RELA gene from RNA-seq results obtained in total cytoplasmic lysates (TOT) or pooled polysomal fractions (POL). **E**) Allelic fraction measurements obtained by Sanger sequencing and electropherogram quantification from independent biological replicates of polysome profiling experiments in HCT116 cells for rs768406925 in RELA. **F**) Correlation between delta allelic fractions measured for the SNPs in the four indicated genes using RNA-seq (Y-axis) or Sanger electropherograms (X-axis). The average and standard deviations of replicates are plotted. **G**) Correlation graph as in F, focusing on the RNA-seq data (Y-axis) and the results obtained by Ampliseq-based targeted resequencing (X-axis).

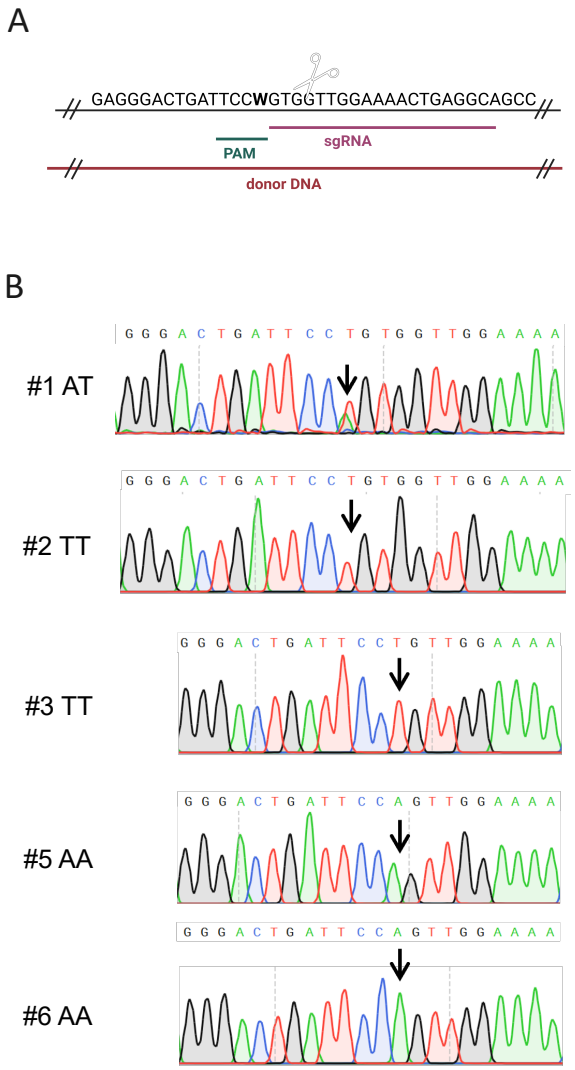

Figure S2. Editing of HCT116 cells to obtain the three genotypes for the rs1053639 T/A SNP.
Parental HCT116 cells - heterozygous for the rs1053639 SNP - were edited to obtain homozygous clones for the A and the T alleles. **A)** CRISPR/Cas9-mediated knock-in was employed for this aim. We annealed a gene-specific crRNA with a tracrRNA, obtaining a sgRNA for DDIT4. The same sgRNA cut both alleles since the SNP represented the "N" base of the -NGG PAM. An 85-nt long donor DNA with the endogenous sequence (mixture of 50% A and 50% T) was purchased to be used as a template. **B)** Representative electropherograms of Sanger sequencing analyses indicating the genotype of the selected clones for rs1053639.

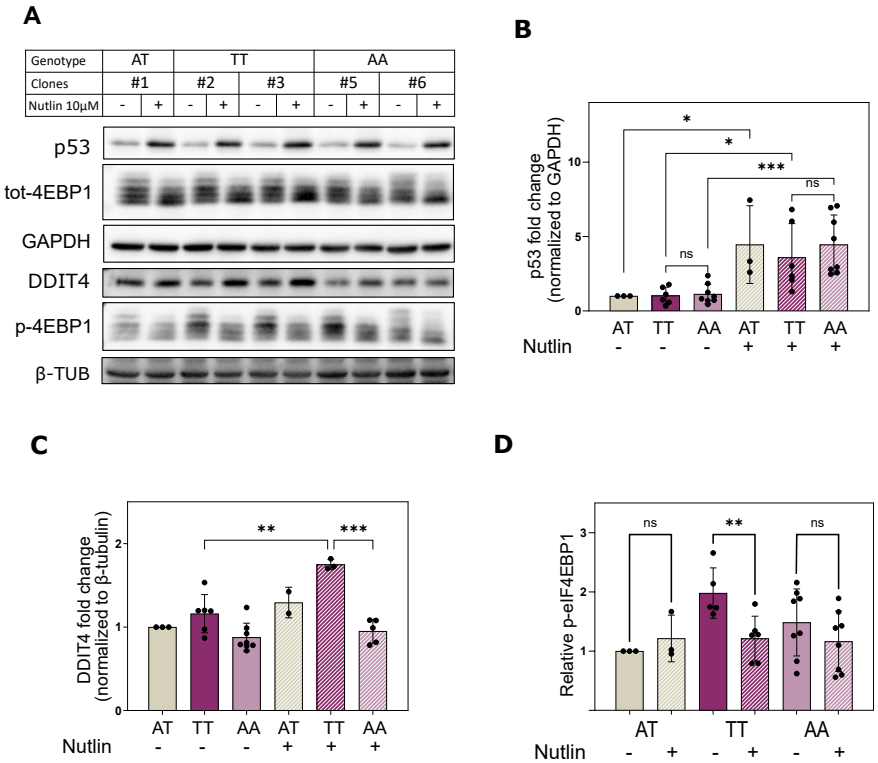

Figure S3. The rs1053639 tranSNP genotype impacts on mTOR pathway markers upon Nutlin. treatment. HCT116 parental cells and clones differing for the rs1053639 homozygous genotypes were treated with either Nutlin 10 µM or vehicle control for 16 hours. **A)** Cell lysates were analyzed by immunoblotting for the induction of p53 and DDIT4 protein levels and the phosphorylation state and levels of the eIF4EBP1 mTORC1 target. β-Tubulin and GAPDH were used as references. **B, C)** Densitometry analysis of p53 and DDIT4 protein levels shows significant induction upon Nutlin treatment. **D)** Densitometry analysis of phosphorylated eIF4EBP1 blots reveals that significant inhibition of the phosphorylation of eIF4EBP1 is apparent only in the rs1053639 TT homozygous clones. ***p-value <0.005. **p-value <0.001. *p-value <0.05. ns, not significant. unpaired t-test.

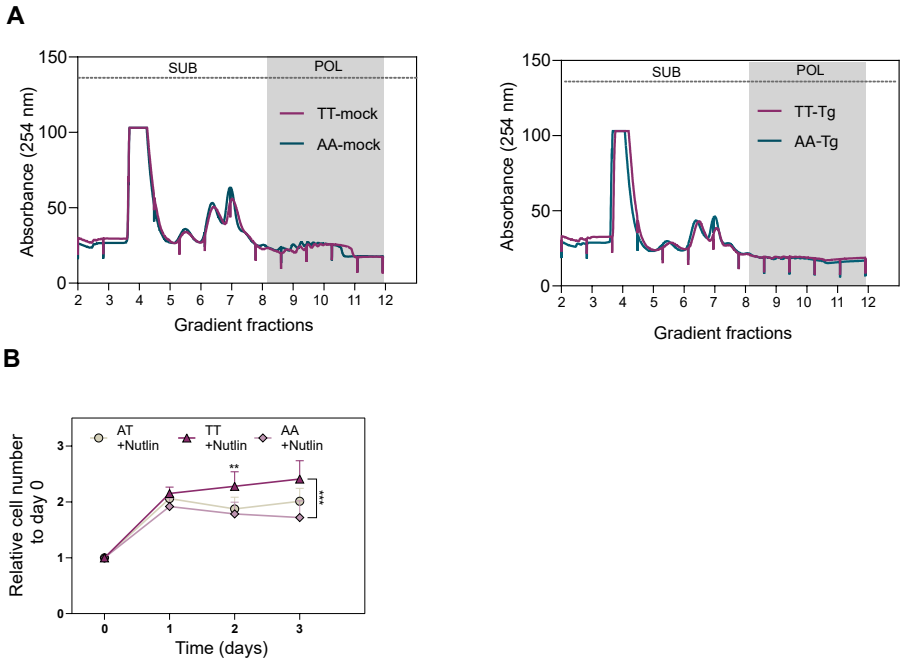

Figure S4. The DDIT4 rs1053639 genotype does not strikingly impact global translation and cell proliferation in response to cellular stresses.

A) Representative polysome profiles of HCT116 TT and AA clones treated with vehicle (Left) or thapsigargin 100nM for four hours (Right). Lysates separated by ultracentrifugation on a linear 15-50% sucrose gradient were fractionated following UV absorbance recorded at 254 nm. The fractions representing RNA complexes used for subsequent analysis are indicated in the figure. **B)** HCT116 cells with the three genotypes differing for the rs1053639 were treated with 5µM Nutlin for 72 hours. The sensitivity of the clones was followed every 24 hours by the Operetta HCS system. Relative cell number curves were plotted as the mean of several replicates ± standard deviation (SD). ***p-value <0.0005. Ordinary two-way ANOVA.

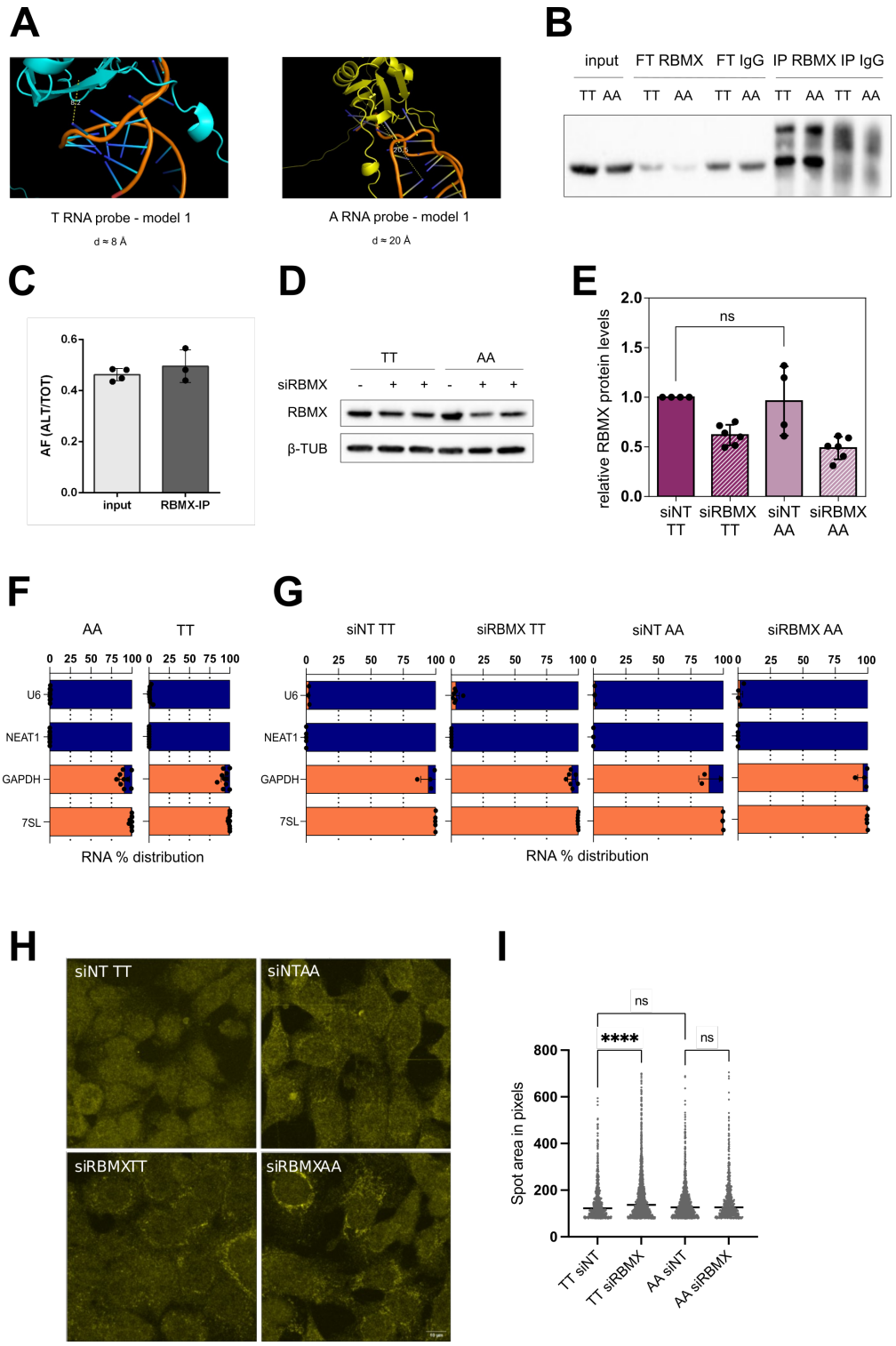

Figure S5. The rs1053639 tranSNP genotype impacts mRNA fate through the RBMX protein.
A) AlphaFold3 was used to predict the interactions between the full-length RBMX protein and the RNA probes (A, T) used for the RNA EMSA. Four models were explored; model 1 is shown as representative. The tool allows the calculation of the

distance between a selected RNA nucleotide and a selected protein portion. The distance between the T SNP nucleotide and the RBMX protein was lower than the distance between the A SNP nucleotide and the same protein in all four models. **B)** RBMX was specifically immunoprecipitated across TT and AA cells with similarly high efficiencies. An IgG control antibody of the same species as the anti-RBMX antibody was used as a control for specificity. FT: flow-through, unbound lysate upon IP. **C)** The endogenous RBMX protein was immunoprecipitated either from a whole cell lysate or from a nuclear extract in heterozygous parental HCT116 cells. RNA from the input and IP samples was extracted and reverse-transcribed. The cDNA was amplified by performing RT-qPCR and submitted to Sanger sequencing. Results are indicated as the AF of the alternative allele (A) over the Total (A+T) and represent the mean ± SD of three independent experiments. **D, E)** TT and AA clones were treated with either a mixture of siRNAs targeting RBMX or the siRNA control for 48 hours. Representative immunoblot and the densitometric analysis show that the RBMX protein is equally expressed independently of the rs1053639 and that the efficiency of RBMX silencing was similar across TT and AA clones. β-Tubulin was used as a loading control. **F)** U6 snRNA and NEAT1 were used as markers of the nuclear fraction, 7SL and GAPDH were used as markers of the cytoplasmic fraction. However, GAPDH mRNA is not completely cytoplasmic, which is consistent with previous reports. Markers for the AA cells are shown on the *left*, and markers for the TT cells are shown on the *right*. **G)** Markers for RNA fractionation upon siNT or siRBMX. U6 snRNA and NEAT1 were used as markers of the nuclear fraction, and 7SL and GAPDH were used as markers of the cytoplasmic fraction. **H)** Confocal images related to Figure 4G: smiFISH of a TT and an AA cell clone after control (siNT) or RBMX depletion, showing only the DDIT4 mRNA, in yellow. Scale bar is 10 µm. **I)** Area of perinuclear, cytoplasmic DDIT4 mRNA spots in pixels. **** $p<0.0001$, ordinary one-way ANOVA. ns = not significant.

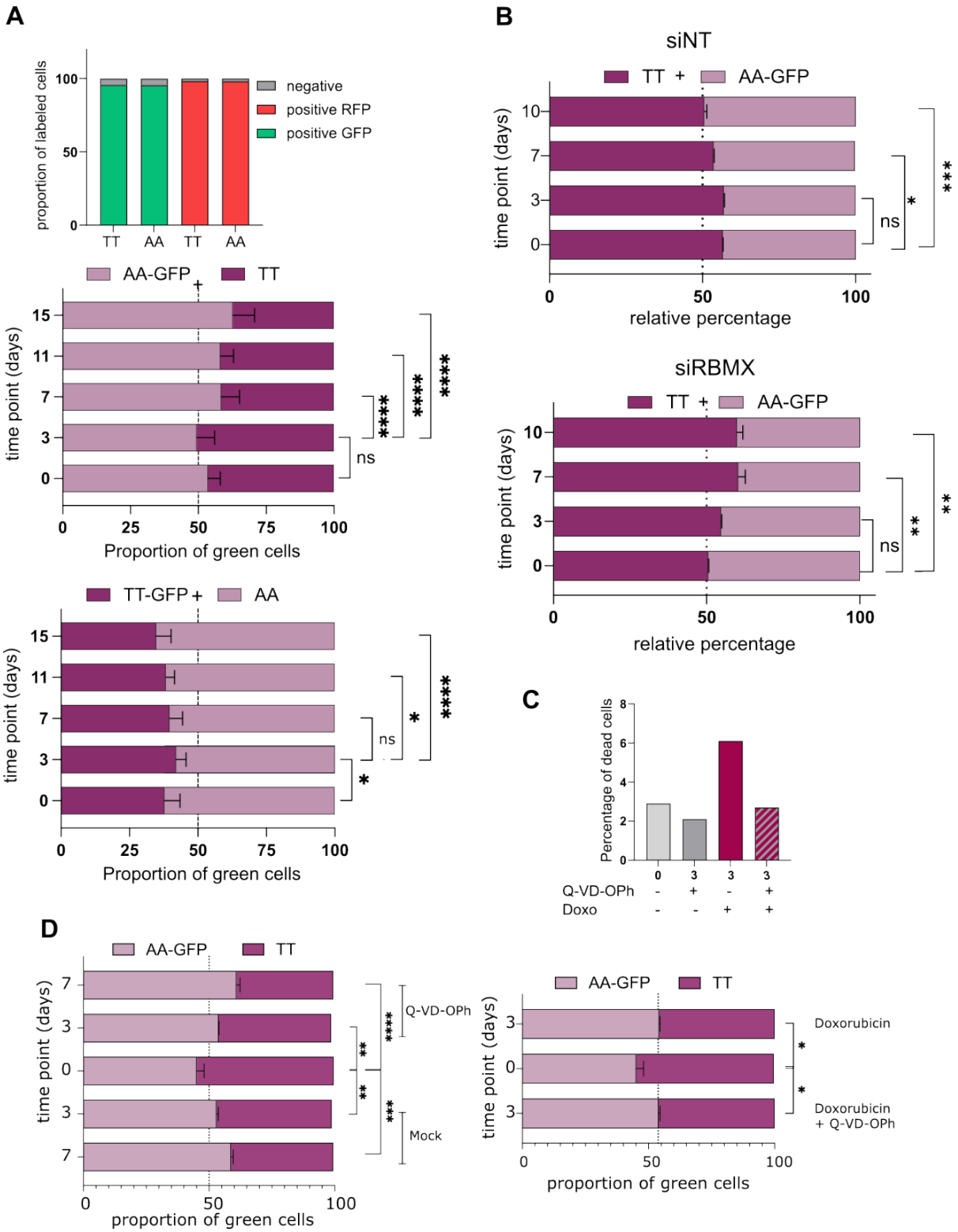

Figure S6. The rs1053639 tranSNP AA genotype shows a competitive growth advantage in prolonged culture conditions.

A) (Top) DDIT4 clones harboring the TT and AA genotypes were both separately transduced with Lentiviral particles to constitutively express either EGFP or MiRFP. After transduction, cells were treated with 5 µg/ml blasticidin for at least 15 days, to reach at least 95% of GFP+ or RFP+ cell populations. (Middle and Bottom) TT and AA clones were co-cultured using both combinations for the fluorophore. The graphs plot the relative proportion of cells and are representative of at least four replicates for each combination. ns = not significant; *p-value < 0.05; ****p-value <0.0001, ordinary two-way ANOVA. **B**) Relative percentage of TT and AA cells at time zero, when the co-culture was started, and at the indicated time points. The relative proportions were calculated by detaching the cells and counting 10,000 events by FACS,

identifying GFP-positive (AA) and GFP-negative cells. At day 0, day 3, and day 7, cells were transfected with a control siRNA (siNT) (Top) or an siRNA targeting RBMX (Bottom). The average relative percentage and the standard deviations of three replicates are shown. The statistical analysis over day 0 is shown. ns = not significant; *p-value <0.05; **p-value <0.001; ***p-value <0.0001, ordinary two-way ANOVA. **C)** HCT116 clones were treated with Doxorubicin (3µM) and/or Q-VD-OPh (10µM) and tested after three days. Percentage of dead cells measured by FACS in the indicated conditions. **D**) The two graphs represent the proportion of GFP+ cells (AA) at day 0 and at the indicated time points of co-culture and treatments. *p-value <0.05; **p-value <0.001; ***p-value <0.0001; ****p-value <0.0001, ordinary two-way ANOVA.

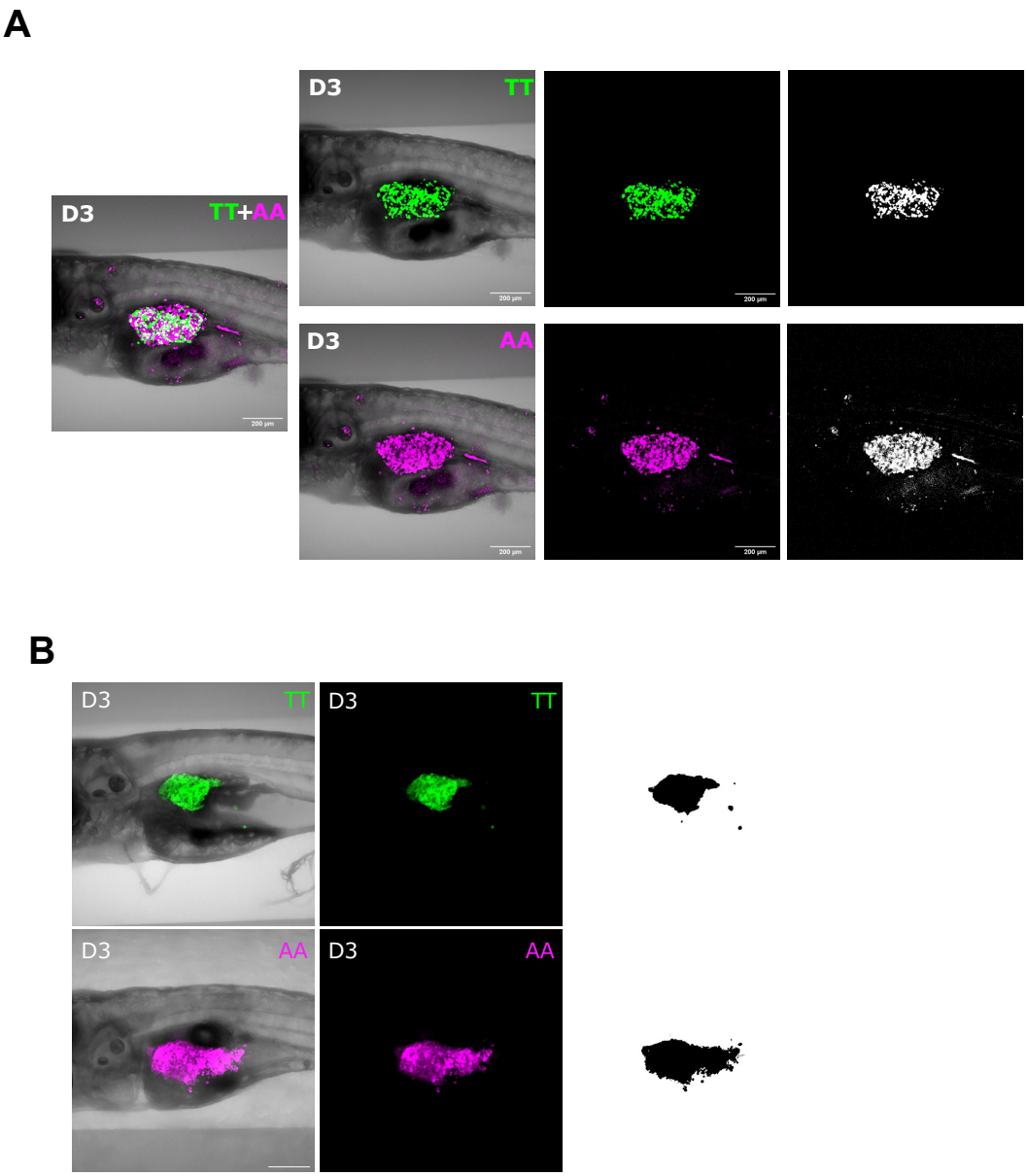

Figure S7. DDIT4 rs1053639 impacts tumor growth and genotypic competition in zebrafish larvae xenotransplants. Image analysis was performed by Fiji software, and quantification of the tumor growth was carried out by applying fixed thresholds for fluorescent intensity, as described in Materials and Methods. **A, B)** Representative images for both confocal and its corresponding Fiji quantification mask.

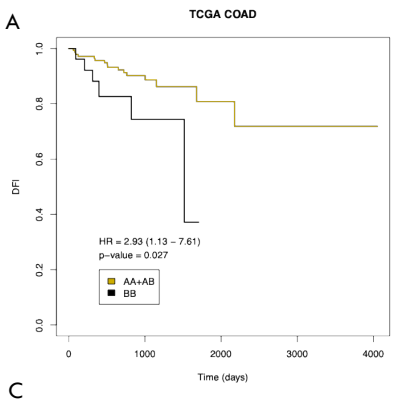

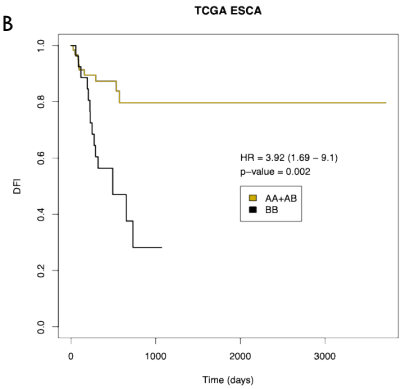

C

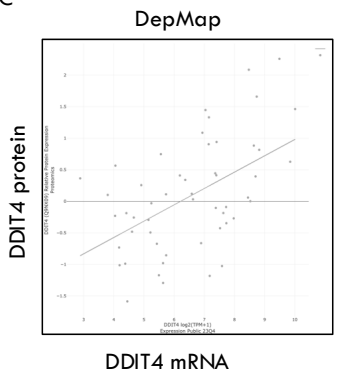

D

IHC score:	High		Low	
	Sample Code	DDIT4 rs1053639 genotype	Sample Code	DDIT4 rs1053639 genotype
Normal Tissue	16-I-04747	TT	16-I-00016	TT
			16-I-02512	TT
			16-I-07061	AT
			15-I-26303	AT
			16-I-14809	AA
			16-I-25747	AA
Tumor Tissue	16-I-04747	TT	16-I-00016	TT
	16-I-14809	AA	16-I-02512	TT
	16-I-25747	AA	16-I-07061	AT
			15-I-26303	AT

E

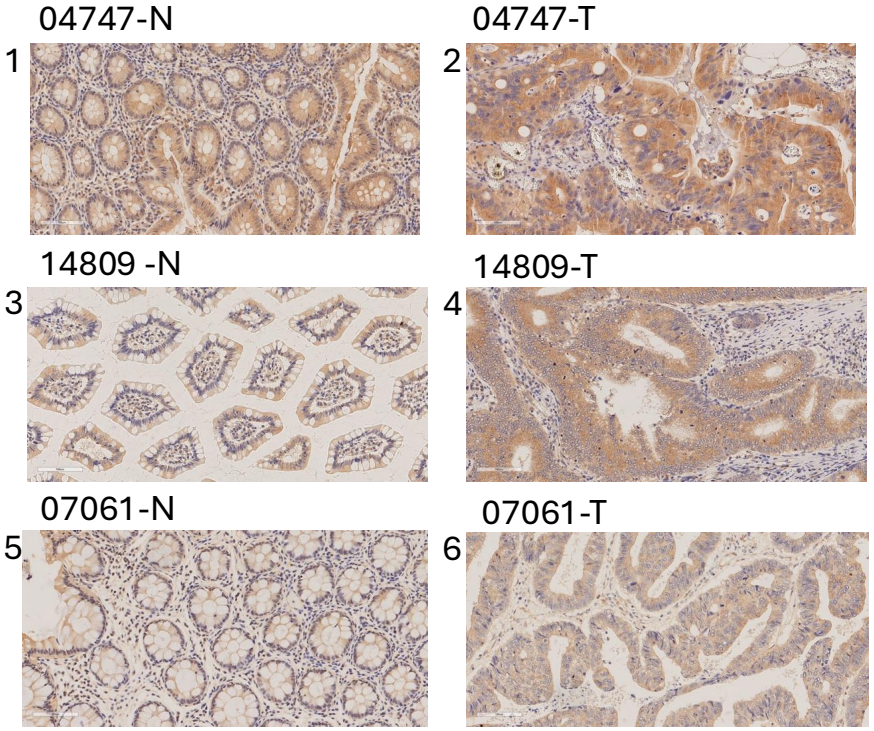

Figure S8. Exploration of the prognostic value of rs1053639 genotype.
A-B) Survival probability from TCGA data plotted after stratifying patients based on the rs1053639 genotype and under a recessive model (A = reference allele (T); B = alternative allele (A)). **C)** Correlation between DDIT4 protein and mRNA levels in cancer cell lines from the DepMap database. **D)** Genotyping results for rs1053639 in seven colon cancer samples. The IHC score was obtained by analyzing the slides by two certified pathologists and applying a custom script in Fiji -see methods-. **E)** Representative images of IHC DDIT4 staining. -N and -T after the sample code refer to normal colon mucosa or cancer tissue, respectively. The sensitivity of IHC staining was verified by paraffin-embedding pellets from our edited HCT116 cell clones (not shown). Images of sample 04747-N and -T, genotype TT, show high expression of cytoplasmic DDIT4 (E1 and E2). Sample 14809-N, genotype AA, shows a low expression of cytoplasmic DDIT4 (E3), while the 14809-

T tumor counterpart shows high expression (E4). Finally, images of sample 07061-N and -T, genotype AT, both show low cytoplasmic expression of the DDIT4 protein (E5 and E6).

List of Supplementary Tables

Table S1. List of analyzable heterozygous SNPs in HCT116 RNA-seq dataset

Table S2. List of the tranSNPs identified. ID, gene name, location, and AF data are reported

Table S3. RNA-binding protein binding predictions for rs1053639.

Table S4. Sequences of primers and siRNAs

Table S5. Sequence of crRNA and donor DNA sequences and summary of the efficiency of the CRISPR/Cas9-mediated HDR.

Table S6. Summary table of the genotypes of selected rs1053639 edited clones.

Table S7. Table of the antibodies used in this study.

Table S8. Comparison of the expression of tranSNP host genes in colon adenocarcinomas and controls, based on TCGA data.